Manuscript prepared for Atmos. Chem. Phys.
with version 4.2 of the LaTeX class copernicus.cls.
Date: 9 June 2015

Source contributions to 2012 summertime aerosols in the Euro-Mediterranean region

Géraldine REA[1], **Solène TURQUETY**[1], **Laurent MENUT**[1], **Régis BRIANT**[1], **Sylvain MAILLER**[1], **and Guillaume SIOUR**[2]

[1]Laboratoire de Météorologie Dynamique, UMR CNRS 8539, Université Pierre et Marie Curie - Paris 6, ENPC, Ecole Polytechnique, Palaiseau, France
[2]Laboratoire Inter-Universitaire des Systèmes Atmosphériques, UMR CNRS 7583, Université Paris Est Créteil et Université Paris Diderot, Institut Pierre Simon Laplace, Créteil, France

Abstract. In the Mediterranean area, aerosols may originate from anthropogenic or natural emissions (biogenic, mineral dust, fire and sea salt) before undergoing complex chemistry. In case of a huge pollution event, it is important to know if european pollution limits are exceeded and, if ~~yes~~so, if the pollution is due to anthropogenic or natural sources. In this study, the relative contribution of emissions to surface PM_{10}, surface $PM_{2.5}$ and total aerosol optical depth (AOD) is quantified. For Europe and the Mediterranean regions and during the summer of 2012, the WRF and CHIMERE models are used to perform a sensitivity analysis on a 50 km resolution domain (from -10°W to 40°E and from 30°N to 55 °N): one simulation with all sources (reference) and all others with one source removed. The reference simulation is compared to data from the AirBase network and two ChArMeX stations, and from the AERONET network and ~~AERONET networks and~~ the MODIS satellite instrument to quantify the ability of the model to reproduce the observations. It is shown that the correlation ranges from ~~0.38 to 0.49~~ 0.19 to 0.57 for surface particulate matter and from 0.35 to 0.75 for AOD. ~~The sensitivity simulations are analysed to quantify the impact of each source.~~ For the summer of 2012, the model shows that the region ~~(from -10W to 40E and from 30N to 55 N)~~ is mainly influenced by aerosols due to mineral dust and anthropogenic emissions (62% and 19% respectively of total surface PM_{10} and 17% and 52% of total surface $PM_{2.5}$). The western part of the Mediterranean is strongly influenced by mineral dust emissions (86% for surface PM_{10} and 44% for $PM_{2.5}$), while anthropogenic emissions dominate in the northern Mediterranean basin (up to 75% for $PM_{2.5}$). Fire emissions are more sporadic but may represent 20% of surface $PM_{2.5}$, on average during the period near local sources. Sea salt mainly contribute for coastal sites (up to 29%) and biogenic emissions mainly in Central Europe (up to 20%).

The same analysis was undertaken for the number of ~~stations in~~ daily exceedances of the European Union limit of 50 μg m^{-3} for PM_{10} (over the ~~AirBase stations)~~stations), and for the number of daily exceedances of the WHO recommendation for $PM_{2.5}$ (25 μg m^{-3}), over the western part of Europe and the central north. This number is generally overestimated by the model, particularly in the northern part of the domain, but exceedances are captured at the right time. ~~The discrepancies are most probably due to an overestimation of dust at the surface, and particularly when diverse sources are mixed. If~~ Optimized contributions computed with the observations show that if natural sources as mineral dust and fire events are particularly difficult to estimate, ~~their contribution to the exceedances of the limitation is preponderant~~ they was responsible exclusively for 35.9% and 0.7% respectively of the exceedances for PM_{10} during the summer of ~~2012 (from 35% in the northern part of the Mediterranean basin to 92.5% in the western part)~~2012. The PM_{25} recommendation of 25 μg m^{-3} is exceeded in 21.1% of the case because of anthropogenic sources exclusively and in 0.02% because of fires. The other exceedances are induced by a mixed contribution between mainly mineral dust (49.5%-67% for PM_{10} exceedances contributions, 4.4%-13.8% for $PM_{2.5}$), anthropogenic sources (14.9%-24.2% and 46.3%-80.6%), biogenic sources (4.1%-15.7% and 12.6%-30%) and fires (2.2%-7.2% and 1.6%-12.4%).

Correspondence to: Géraldine REA
(geraldine.rea@lmd.polytechnique.fr)

1 Introduction

Numerous studies have shown the deleterious impact of particulate matter (PM) air pollution on human health. In particular, small particles, PM_{10} and $PM_{2.5}$ (particulate matter with an aerodynamic diameter lower than 10 and 2.5 μm, respectively), enhance cardiopulmonary mortality and mor-

bidity (Katsouyanni et al., 1997; Boldo et al., 2006; Pope III and Dockery, 2006) due to their deeper penetration into the respiratory system.

Beyond these concerns, aerosol quantification is needed to evaluate its contribution to climate change. PM have a direct impact due to the absorption and scattering of solar radiation, the so-called "aerosol direct effect", as well as an indirect impact due to their role as cloud condensation nuclei (Yu et al., 2006; Carslaw et al., 2010; Stocker et al., 2013). Absorbing aerosols have also a "semi-direct effect" on cloud evaporation and cloud cover (Hansen et al., 1997).

Monitoring particulate matter ambient concentrations is thus an important issue for regional air quality and climate, and has become a key concern for pollution regulations in the past decade. Therefore, a correct understanding and quantification of aerosol formation and evolution is required.

The Mediterranean region is heavily influenced by numerous anthropogenic and natural aerosol sources and is often exposed to air pollution (Monks et al., 2009). Those sources, combined with complex interactions between atmospheric dynamics, geographic features and land-sea temperature gradients (Lionello et al., 2006), lead to an European aerosol load maximum (Textor et al., 2006; Putaud et al., 2010). Meteorological conditions hold a key role in the development of aerosol-related pollution events (Millán et al., 2002). Being in a transitional zone between the subtropical high-pressure belt and the mid-latitude westerlies and low pressure systems, the Mediterranean region is characterized by hot, dry summers and mild, wet winters. These meteorological patterns govern the transport of aerosols released from various sources around the Mediterranean region and lead to a maximum aerosol load during the summer (Monks et al., 2009; Nabat et al., 2013). Moreover, a mixture of different sources is usually observed due to the long-range transport of the associated particles (DallOsto et al., 2010; Gerasopoulos et al., 2011; Boselli et al., 2012). Due to these complex characteristics, the specific impact of each aerosol source cannot be easily assessed.

The region is impacted by local emissions from anthropogenic activities and by biogenic emissions of precursors of aerosol formation. Most of $PM_{2.5}$ exceedances are due to primary pollution but these are enhanced by the production of secondary aerosols (Koçak et al., 2007). For instance, Sartelet et al. (2012) found that Secondary Organic Aerosol (SOA) formation over Europe is strongly impacted by biogenic emissions (72-88%) in addition to anthropogenic emissions of precursors. Another study by Im and Kanakidou (2012) showed that regional anthropogenic emissions contributes to 47% of $PM_{2.5}$ in the Eastern Basin (Greece, Turquey) in summer, with 4% from Istanbul.

Moreover, the long-range transport of mineral dust from North Africa significantly affects PM concentration throughout the region. Several studies of available observations show that the PM_{10} European Union air quality standard (50 μg m^{-3}, daily average) is exceeded at many ~~location~~ locations around the basin because of ~~mineral dust in addition to local anthropogenic pollutants~~ a combination of mineral dust and anthropogenic pollutants from local sources (Gerasopoulos et al., 2006; Gobbi et al., 2007; Koçak et al., 2007; Rodriguez et al., 2007; Kaskaoutis et al., 2008). Mineral ~~mineral~~ dust outbreaks, although transported through the Mediterranean sea during all seasons, are more frequent in spring and summer, where dust plumes are transported through the Atlantic and reach mainly and regularly the western part of the region (Moulin et al., 1998; Israelevich et al., 2012; Salvador et al., 2014; Ripoll et al., 2015). In summer, mineral dust aerosols are also observed over central Europe (Israelevich et al., 2012; Salvador et al., 2014).

Another important source of PM in the Mediterranean basin is sea salt, which can account for instance in Erdemli (Eastern Mediterranean) for up to 50% of PM_{10} ~~pollution~~ concentration thresholds exceedances (Koçak et al., 2007).

Vegetation fires (recurrent in eastern and southern Europe during ~~Spring and Summer~~spring and summer) are also a significant additional source of PM (Turquety et al., 2014), with consequences on air quality throughout the basin (Pace et al., 2005; Hodzic et al., 2007; Barnaba et al., 2011).

The natural emissions from fires and mineral dust are particularly difficult to quantify accurately due to their intense and sporadic nature resulting in large spatial and temporal variability. Several projects have been undertaken over the past years to improve the understanding and the quantification of particulate pollution over the Mediterranean region. Among those, the ChArMEx international program (Chemistry-Aerosol Mediterranean Experiment, *http://charmex.lsce.ipsl.fr*), allowed the settlement of several additional observation sites as well as intensive measurement campaigns during the summers of 2012, 2013 and 2014. In 2012, the ChArMEx/TRAQUA (TRansport and Air QuAlity) experiment allowed the characterization of a very intense dust transport event measured at the end of June over the Western Mediterranean (Nabat et al., 2015). In addition, several large fires were reported during the summer of 2012, more particularly in the Balkans (Anttila et al., 2015) and in Spain ~~, where $PM_{2.5}$ reached 160 μg m^{-3} at Burjassot (Valencia)~~ in July (Gómez-Amo et al., 2013).

The majority of the studies previously cited have been made at specific experimental sites and sometimes for specific case studies or sources. The purpose of our analysis is to estimate the relative contributions of this diversity of sources, and thus to draw a regional context of aerosol pollution during the summer of 2012 in the framework of the ChArMEx program.

Aerosol optical properties are important to characterize aerosols for air pollution monitoring. They are needed to estimate the radiative effects, which have themselves an impact on photochemistry by modifying the photolysis rates (Mailler et al., submitted). Moreover, optical properties are directly related to aerosol particle concentration, type and size. The observations of aerosol optical properties

from remote sensing instruments thus provide an important complement to the surface PM databases. In particular, extensive measurements of the Aerosol Optical Depth (AOD), characterizing the light extinction associated with the aerosols along the full vertical column, are provided by the surface AErosol RObotic NETwork (AERONET; *http://aeronet.gsfc.nasa.gov*) and by several satellite-based instruments, allowing a very good spatial and temporal coverage.

In addition to the analysis of surface and remote sensing observations, chemistry-transport models (CTMs) are required for the simulation of atmospheric composition and the understanding of physico-chemical processes. Model validation or inter-comparisons have shown that, although the modelling of ozone or other gases has been improved in the past years, the modelling of PM is still a concern, with a persistent underestimation of PM_{10} for the majority of the CTMs (Roustan et al., 2010; Solazzo et al., 2012; Im et al., 2014). Moreover, $PM_{2.5}$ is also overestimated when PM_{10} is improved, although the biases on $PM_{2.5}$ are lower than those on PM_{10}. Even though emissions probably constitute a significant source of uncertainty, the uncertainty in modelled PM concentrations linked to the parameterization choices (vertical diffusion, number of levels, deposition, etc.) and to the meteorological fields can be for instance higher than the uncertainty linked to PM anthropogenic and biogenic emissions (Sartelet et al., 2012). The uncertainty on PM concentrations leads to uncertainties on the simulated aerosol optical properties and AOD (Péré et al., 2010; Curci et al., 2014), in addition to uncertainties in the calculation of optical properties (refractive indices, assumptions on aerosol mixing, density).

This paper provides an analysis of the main contributions of aerosol sources to both surface PM and Aerosol Optical Depth (AOD) in the Mediterranean region using the state-of-the-art regional CTM CHIMERE (Menut et al., 2013). ~~The majority of the studies previously cited have been made at specific experimental sites and sometimes for specific case studies.~~ This paper aims at estimating the contribution of each source in Europe and the Mediterranean Basin, to provide a description of the zones of influence of given sources on regional air pollution.

After an evaluation of the model's performance through comparisons to observations from surface networks and remote sensing, a sensitivity analysis is conducted on the case study of the summer of 2012 (June-July-August). This time period allows an analysis including all sources (fires and dust outbreaks notably occurred during this period). Estimations of the relative contributions of the main aerosol sources to the aerosol load in the Mediterranean area is provided. Section 2 describes particulate pollution during the summer of 2012 based on the available observations of surface PM and AOD. Section 3 presents the tools and methodology used in this paper. The model is evaluated against observations in section 4, and sensitivity simulations are discussed in section 5 and 6, where an estimation of contributions to surface PM and AOD and to air quality threshold exceedances is also assessed.

2 Presentation and analysis of observations

Aerosol quantification from 1st June to 31 August over the region is analyzed in this section using observations of both surface PM concentrations and AOD, which provide an overview of the main polluted regions and the temporal variability of aerosol concentrations.

2.1 Surface PM

Surface PM concentrations from the model are evaluated through comparisons to $PM_{2.5}$ and PM_{10} observations from the European Air quality database (AirBase) of the European Environment Agency (*http://acm.eionet.europa.eu/databases/airbase*). This database provides air quality monitoring data and information from 38 countries around Europe, and includes more than 6000 stations providing hourly and daily measurements. The diversity of instruments and sampling, associated with certain meteorological conditions (humidity) contribute to the uncertainty of the database. The quality standards on the measurements for the AirBase network is less than 25%. Only rural and background stations are included in the present paper. Indeed, urban sites being strongly influenced by local sources, they are not relevant for this analysis of the regional trends and budget of pollution. This reduces the number of stations to ~~760~~ 927 for PM_{10} and ~~161~~ 316 for $PM_{2.5}$. Two additional rural stations located in Corsica in the frame of the ChArMEx project are also taken in consideration (Venaco and Ersa).

The average concentration from 1 June to 31 August 2012 at the ~~AirBase~~ PM_{10} stations is shown in Figure 2~~.~~, with the number of days with data shown on Figure 1. Almost all stations present data every day of the studied time period. Most of the stations are concentrated in the central north of the domain, so that the analysis over the Mediterranean Sea itself and around most of its coasts is not possible.

The observations show that some regions are recurrently affected by pollution. These correspond to most of the Mediterranean coastline (stations in Spain, South of France), with monthly averaged concentrations of PM_{10} up to 40 μg m^{-3} and maxima around 200 μg m^{-3}. The Po Valley and the Benelux are also affected by high levels (up to 200 μg m^{-3}) as well as Eastern Europe.

For example, high values of PM are detected in Farollilo near Salamanca, Spain (Figure 3) at the end (27-28) of June (with a concentration up to 120 μg m^{-3}), and end of July and above 80 μg m^{-3} during August (around the 10 and 18-19). The level of PM in this area remains high (around 40 μg m^{-3} for daily mean) during the whole time period. Observations in the South of France show lower temporal variability with

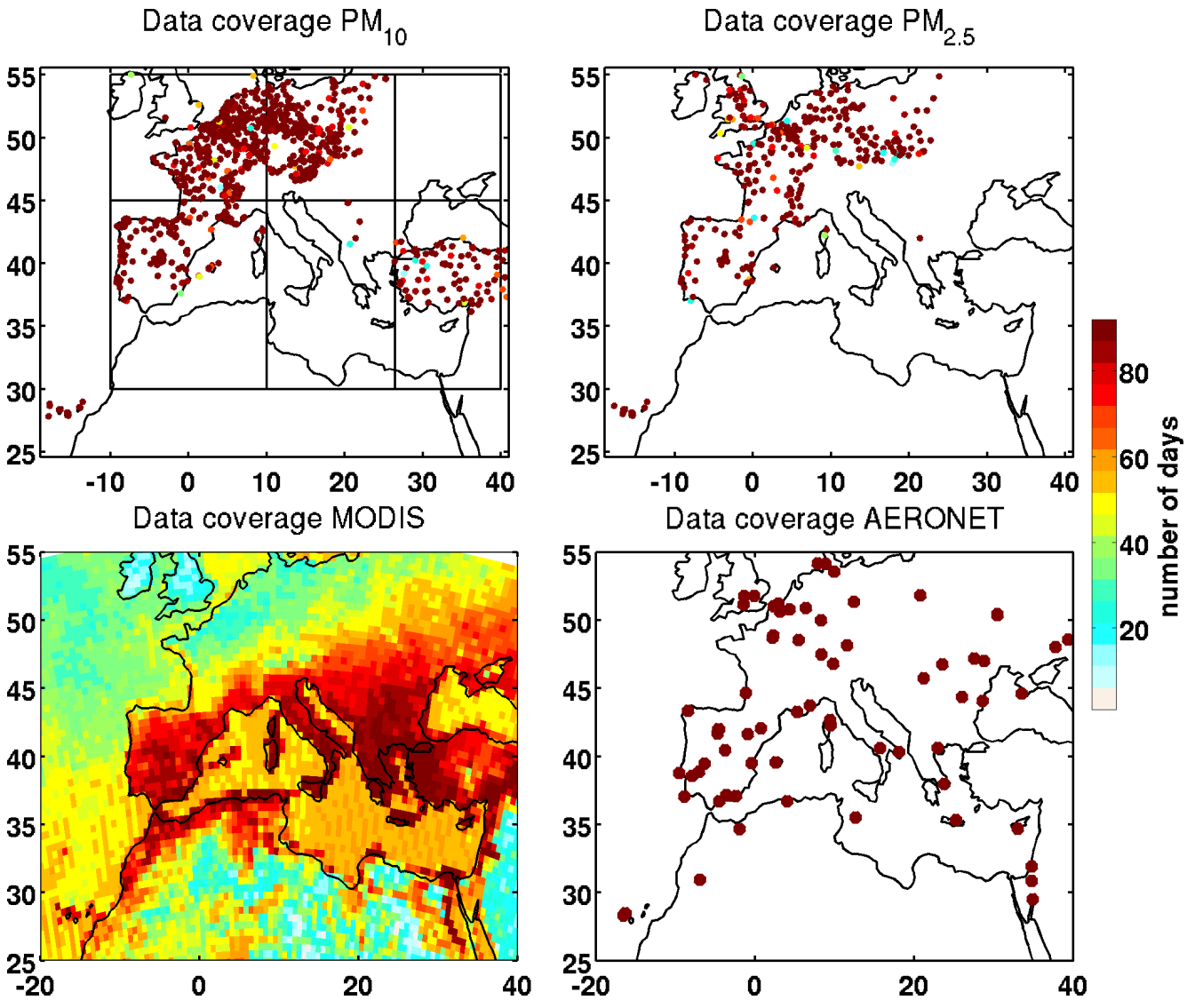

Fig. 1. *Data coverage during the summer of 2012 (1st June to 31 August, 92 days) for each observation dataset, i.e. number of days with measurements from AirBase stations with PM_{10} and $PM_{2.5}$ values, AERONET stations and MODIS data with values for the AOD at 500 and 550nm, respectively.*

concentrations from 10 to around 50 μg m^{-3}. Some sporadic hourly values (not shown) reach more than 100 μg m^{-3} around the 20-21 June, at the end of July and the end of August. For example, at the station located in Miramas in South of France, hourly values reach more than 250 μg m^{-3} (daily mean value of 80 ~~of the daily mean values~~μg m^{-3}) around the 20 June, during the end of July, and during the beginning of August.

Eastern Europe is also affected by high concentrations, as shown for example by the Lomza station in Poland, with peak values around the 30 June (up to 90 μg m^{-3}), at the end of July (above 300 μg m^{-3} for Mragowo, Poland) and during the second half of August (up to 100 μg m^{-3}).

2.2 Aerosol optical depth (AOD)

In addition to surface PM, remote sensing observations of AOD, which provides information on the column integrated aerosol load, are analysed. Both surface remote sensing from AERONET and satellite observations from the Moderate Resolution Imaging Spectroradiometer (MODIS) are used.

AERONET is an optical ground-based aerosol-monitoring network, composed of spectral radiometers. It allows measurements of AOD every 15 min at 8 wavelengths (centred between 340 and 1020 nm). With more than one hundred stations in the world, the network is widely used for the vali-

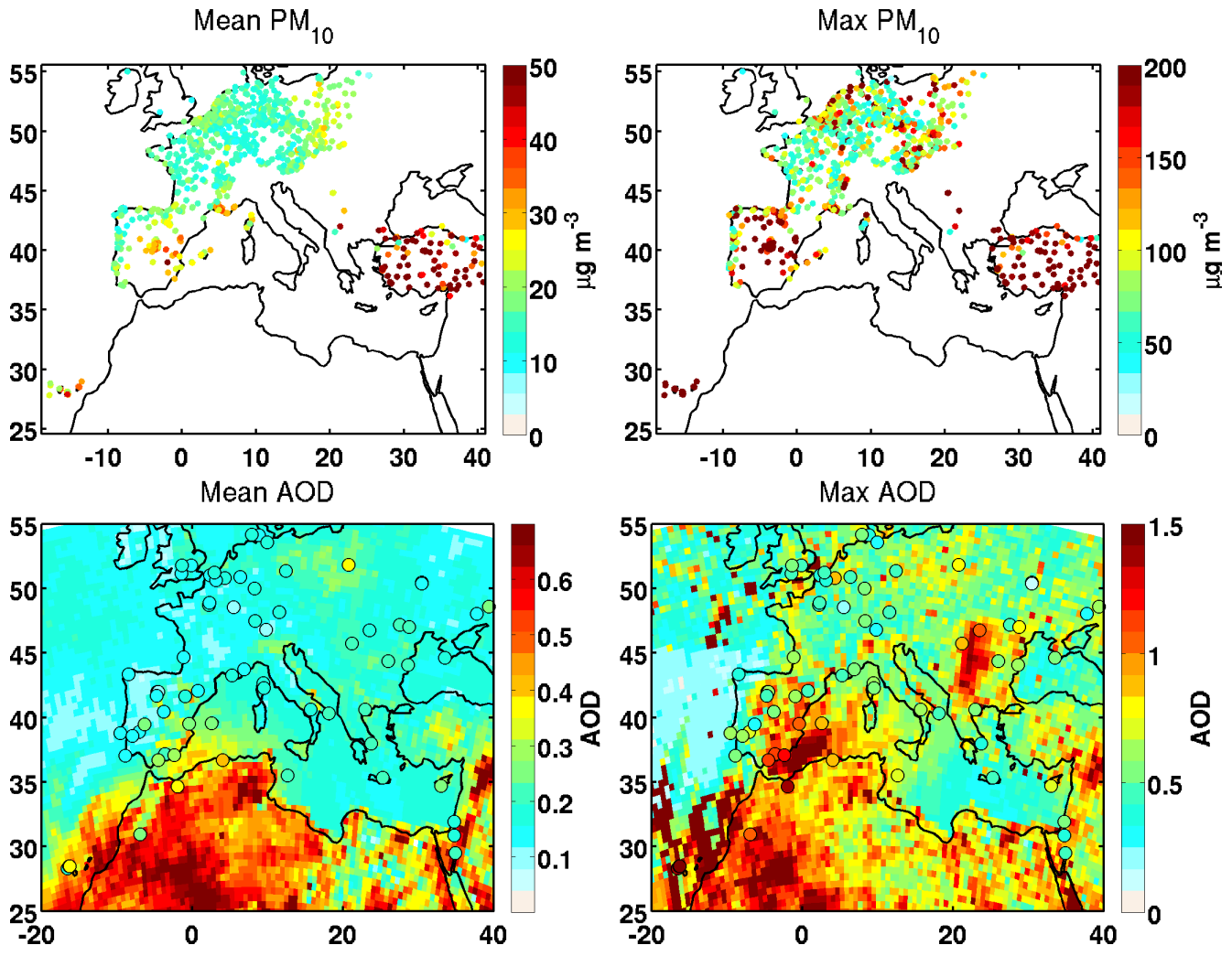

Fig. 2. *Summer 2012 (1st June to 31 August) daily average for surface PM_{10} concentrations from the AirBase network and Ersa and Venaco stations (upper left) and Aerosol Optical Depth at 550 and 500 nm respectively from MODIS instrument and AERONET stations (bottom left). Daily maximum over the period is shown on upper right panel for surface PM_{10} concentrations and bottom right panel for Aerosol Optical Depth.*

dation of model simulations and satellites observations. The main product examined here is the total AOD at 500 nm from the level 2.0 cloud screened and quality assured retrievals of the ground based AERONET sun photometers.

The estimated precision of the direct AOD measurements is ∼0.01 (at 440 nm) for a recently calibrated instrument (Holben et al., 1998), and the uncertainties are well-documented (Dubovik et al., 2000). During the period of the simulation and within the domain, data from 53 stations of the network are available, with values each day of the summer of 2012 (Figure 1). Their location is shown in Figure 2.

Surface site measurements do not allow a full regional evaluation, particularly around the Mediterranean Basin, which is poorly covered. Satellite observations therefore offer a good complement. MODIS is carried on board the Terra and Aqua satellites (NASA) and enables a daily near-global coverage of the Earth with its large swath of almost 2330 km. The satellites cross the equator at about 10:30 and 13:30 (ascending node) respectively. The measurements over 36 spectral bands (from 0.41 to 15 μm) allow the retrieval of many aerosols properties. For this study, the aerosol products MOD04 (for Terra) and MYD04 (for Aqua) L2 5.2 collection data are used (Remer et al., 2006). It includes daily AOD at 550 nm, as well as the Deep-Blue AOD (Sayer et al., 2013) that provides AOD over bright land areas (especially useful here for North Africa). They are available at 10 km$\times$10 km resolution. The expected error for the AOD is $\pm 0.05 \pm 0.15\tau$ over land and $\pm 0.03 \pm 0.05\tau$ over ocean, with a good agreement with ground based measurements (Remer et al., 2005).

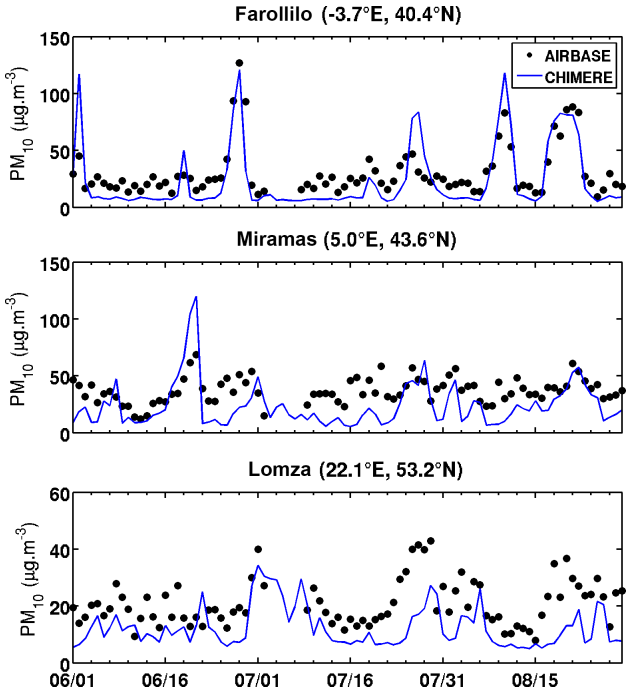

Fig. 3. *Time series from 1st June to 31 August of daily mean surface PM_{10} concentrations from 3 stations of the AirBase network. First station is located near Salamanca in Spain, second is in Miramas in South of France, and third is in Lomza in Poland. The corresponding simulated CHIMERE concentrations (spatially co-localized) are also indicated (blue line).*

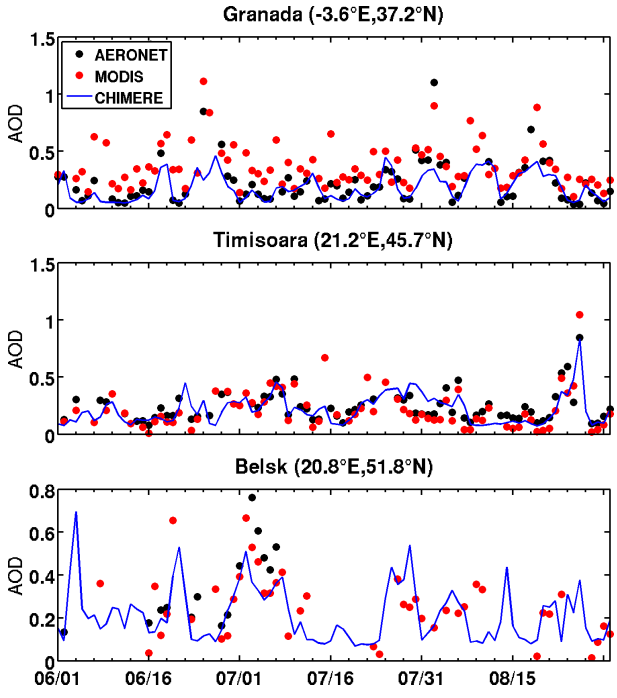

Fig. 4. *Time series from 1st June to 31 August of the daily AOD at 500 nm from three AERONET stations. First station is Granada in Spain, second is Timisoara in Romania, and third is Belsk in Poland. Values from MODIS at 550 nm are also indicated in red dots at these stations, as well as the simulated spatially co-localized 550 nm AOD from CHIMERE (blue line).*

The data coverage over the studied time period is shown on Figure 1. The Mediterranean Basin presents AOD values almost every day. For Eastern Europe and the Balkans, fewer AERONET or AirBase stations are available. The North of Europe is under-represented during the period, due to recurrent clouds in the area.

The AOD at 550nm from the AERONET and MODIS datasets have been compared over the studied region and time period. Both datasets are coherent in variability and levels: correlation coefficients range from 0.71 in MED-Ea to 0.96 in NEU-We and there is a slight overestimation of MODIS compared to AERONET measurements (mean fractional bias of 7% on average).

Spatial patterns of AOD over the region are similar to the ones observed in terms of surface PM concentrations (Figure 2, bottom right panel), with high values at the south of the domain (up to 2 for North Africa and all around the Mediterranean Sea on a seasonal average), the Po Valley and Northern Europe (up to 1.2). MODIS allows a better coverage ~~then~~ than surface measurements in some regions, like North Africa, the Mediterranean Sea, the Atlantic Ocean, the Balkans and the eastern part of the domain (Eastern Europe, Middle East, etc.) For example, large values of AOD, from 1 to 2, are observed with MODIS in the Balkans.

Time series for three AERONET stations are shown in Figure 4. Clear enhancements are detected above Granada at the end of June (19 and 25-26 June), and in August (2nd of August, 8-9 and 18). The Timisoara station shows values around 1 on the 24 of August for both MODIS and AERONET. Finally, observations at Belsk in Poland show lower values but a notable peak around 1 July.

A comparison of these AOD observations for 2012 against the climatology from Nabat et al. (2013), which includes the AOD from 2003 to 2009 using both model and satellite-derived AOD products, indicates that this summer was in the average regarding the aerosol load. Exceptions appears in June where the AOD was higher than the climatology in North Africa and over the Atlantic Ocean near North African coasts (due to a strong dust event (Nabat et al., 2015)), and in August with high values over the Balkans and over the Mediterranean close to the Spanish coastline. There are also higher punctual values in Spain in July. This comparison shows that the period was affected by air pollution from different sporadic events.

From this analysis, several regions and time periods with enhanced aerosol concentrations are identified during the summer of 2012. North Africa and the western Mediterranean Basin were regularly affected by the highest aerosol

loads, with extreme peaks around 26 June and three times in August (daily mean of around 130 μg m^{-3} for PM_{10} and AOD around 1). Eastern Europe appears to show other influences with high concentrations of surface PM at the end of June, the end of July and the end of August (daily mean of 40 μg m^{-3} for PM_{10}, AOD up to 0.8). In the Balkans, MODIS also observed relatively high AOD (around 1) at the end of August.

For the rest of this study, the domain was divided into six sub-regions, which present different characteristics in terms of sources, population density as well as meteorological patterns, which are reflected in the observations. The acronym MED and NEU represent respectively all the Mediterranean Basin and the northern European part of the domain. MED and NEU regions are divided into western, central and eastern zones (MED-We, MED-Ce, MED-Ea and NEU-We, NEU-Ce, NEU-Ea). The delimitation of the regions are indicated in Table 1 and Figure 2.

3 Modelling tools

The sensitivity of aerosol concentrations in the region to each source is evaluated using the CHIMERE regional CTM, driven by meteorological simulations performed using the mesoscale non-hydrostatic Weather Research and Forecasting (WRF) model.

The analysis is focused on the summer of 2012 (1 June to 31 August 2012), with a 10-d spin-up. The simulation domain is chosen to include all contributing sources around the basin (including North Africa until Sahel, a part of the Atlantic Ocean, Eastern and Northern Europe). A Lambert conformal projection is used with a constant horizontal resolution of 50 km $\times$ 50 km. The domain is represented on Figure 5.

This section introduces the models used, their configuration for this analysis, the emissions databases as well as the numerical approach used.

3.1 The WRF meteorological model

The meteorological fields are simulated using the WRF model version 3.5.1 (Skamarock et al., 2008), on a 50 km horizontal grid (same horizontal domain described above). The simulation has been performed with boundary conditions and nudging from the meteorological analysis data of NCEP (Kalnay et al., 1996), provided on a regular $1.125^o \times 1.125^o$ grid.

The model is used in its non-hydrostatic configuration. The vertical grid covers 30 levels from the surface to 50 hPa. The WRF Single-Moment 6-class (Hong and Lim, 2006) is used for microphysics, and RRTMG (Iacono et al., 2008) and the Dudhia schemes (Dudhia, 1989) are used for long and short wave radiation respectively. The surface layer scheme is based on the Monin-Obukhov scheme (Janjic, 1996). Surface planetary boundary layer physics use the Noah Land Surface Model and Yonsei University scheme and the cumulus parameterization is based on the Kain-Fritsch scheme (Kain, 1993).

The WRF simulation outputs are then interpolated on the vertical resolution of CHIMERE and used to diagnose additional parameters (e.g. boundary layer height, friction velocity). Both meteorology and chemical concentration output fields are provided at 1 hour time intervals.

3.2 The CHIMERE chemistry-transport model

CHIMERE is an off-line regional CTM forced by emissions (see section 3.3), meteorological fields (see section 3.1) and boundary conditions. The model version chimere2014 (Menut et al., 2013) is used here on the 50 km horizontal resolution grid described above. The vertical discretization consists in 18 uneven levels in hybrid sigma-pressure coordinates, from the surface up to ~~200hPa~~200 hPa and with 8 levels under 800 hPa.

The reduced chemical mechanism called MELCHIOR2 is used here and includes 44 species involved in almost 120 reactions. The list of species and reactions is provided in Menut et al. (2013). The aerosol module developed by Bessagnet et al. (2004) allows the simulation of primary particulate matter and secondary species: nitrates, sulphates, ammonium, primary organic matter (POM), secondary organic aerosol (SOA), elemental carbon (EC), marine aerosols and mineral dust. Their life cycle is represented with a complete scheme of nucleation, absorption, adsorption, desorption, coagulation, as well as wet and dry deposition and scavenging. The size distribution is simulated using a sectional representation, i.e using five bins from a diameter of 40 nm to 40 μm.

Initial and boundary conditions are provided by 5 years monthly-averaged simulations by the global model LMDZ-INCA for aerosols and trace gases (Folberth et al., 2006), and GOCART for mineral dust (Ginoux et al., 2001).

The photolysis rates are calculated online using the Fast-JX module, version 7.0b (Wild et al., 2000; Bian et al., 2002) as described in Menut et al. (2013). The module computes the actinic fluxes by resolving the radiative transfer in the modelled atmospheric column. The treatment of optical properties is made by taking into account absorption by tropospheric and stratospheric ozone, Rayleigh scattering, absorption by aerosols, and Mie diffusion by aerosols and by liquid- and ice-water clouds. The total AOD is also obtained from these calculations, with an internal mixing state assumption for aerosols, at five different wavelengths: 200, 300, 400, 600 and 1000 nm (Mailler et al., submitted). As the calculation of the photolysis rates is performed at each physical time step taking into account the actualized concentrations of ozone and aerosols, this methodology allows retroaction of aerosol and ozone concentrations on photochemistry. In this study, the simulated AOD from CHIMERE at 500 and

Table 1. *Coordinates of the simulation domain and sub-domains used for further analysis.*

Domain	Acronym	Longitude (°E)		Latitude (°N)	
		minimum	maximum	minimum	maximum
Full domain		-52.6	68.6	-4.3	56.4
Northern Europe - West	NEU-We	-10.0	10.0	45.0	55.0
Northern Europe - Centre	NEU-Ce	10.0	26.0	45.0	55.0
Northern Europe - East	NEU-Ea	26.0	40.0	45.0	55.0
Mediterranean Basin - West	MED-We	-10.0	10.0	30.0	45.0
Mediterranean Basin - Centre	MED-Ce	10.0	26.0	30.0	45.0
Mediterranean Basin - East	MED-Ea	26.0	40.0	30.0	45.0

550 nm are used and extracted ~~by a linear interpolation~~ using the Angström coefficient from the output wavelengths.

3.3 Emissions

This section briefly describes the databases used for both primary particulate matter emissions and the emission of gaseous precursors.

Anthropogenic emissions are the only emissions that can be controlled; their inventories are updated constantly to take into account precise emissions in scenario studies. In this paper, the EDGAR-HTAP_V2 inventory for the reference year 2010 is used. It uses HTAP (Hemispheric Transport of Air Pollution) annual total masses which includes nationally reported emissions combined with regional scientific inventories, complemented with EDGARv4.3 data (*http://edgar.jrc.ec.europa.eu/htap_v2*). The inventory provides global annual emissions for CH_4, NMVOC, CO, SO_2, NOx, NH_3, PM_{10}, $PM_{2.5}$, BC and OC, with a resolution of $0.1° \times 0.1°$. The annual emitted masses are disaggregated into model species and mapped onto the specified grid. Hourly emissions are estimated by applying seasonal, daily and weekly factors depending on the SNAP (Selected Nomenclature for Air Pollution) sectors (Menut et al., 2012). Anthropogenic emissions represent 90 to 100% (among all other sources) of the regional emissions of NOx, NH_3 and SO_2, which are important precursors of inorganic aerosol formation. For example, the total fluxes of NOx in the region for the summer of 2012 are shown in Figure 5. Anthropogenic emissions also amount to 53% of primary organic matter emissions, 81% of black carbon emissions, and 74% of other primary particulate matter emissions.

Biogenic emissions fluxes are calculated using the global Model of Emissions of Gases and Aerosols from Nature (MEGAN; Guenther et al., 2006) and affect six CHIMERE species (isoprene, α-pinene, β-pinene, limonene, ocimene and NO). MEGAN is based on canopy-scale emission factors depending on the species. In their analysis of isoprene emissions over Europe, Curci et al. (2010) compared CHIMERE simulation to satellite observations and found that MEGAN isoprene emissions might be 40% higher over the Balkans, 20% too high over Southern Germany, and 20% too low over Iberian Peninsula, Greece and Italy. In Figure 5, showing the calculated total biogenic fluxes of VOCs in Europe and the Mediterranean Basin during the summer of 2012, we can see that the majority of the emissions fluxes are located in the Balkans and Eastern Europe, and in general in the northern European part of the domain.

Mineral dust emissions use fluxes calculation with the Marticorena and Bergametti (1995) parametrisation for saltation and the optimized dust production model (Alfaro and Gomes, 2001; Menut et al., 2005) for sandblasting. The dust production model uses the model presented in Menut et al. (2013), which has been extended to be applicable to any region and not just North Africa (Briant et al., 2014). It uses new global soil and surface input datasets along with the global ASCAT/PARASOL aeolian roughness length dataset (Prigent et al., 2012). Parameterizations for humidity (Fecan et al., 1999) and seasonal vegetation variation were included. Since long-range transport from North Africa affects strongly the Mediterranean basin and Europe, the simulation domain was chosen in order to include western Africa and the Sahel, known to be active mineral dust sources (Israelevich et al., 2002; Prospero et al., 2002). On Figure 5, representing the mineral dust emissions computed for the study, the majority of them are located in this region. Mineral dust particles are chemically inert in CHIMERE, but their size distribution is affected by wet and dry deposition. Dust emissions and deposition are strongly affected by meteorological fields, leading to large uncertainties (Menut et al., 2007, 2009).

Fire emissions are calculated using the APIFLAME v1.0 emissions model, described in Turquety et al. (2014), with a classical approach of multiplying the burned area by the fuel load consumed and the emission factors specific to the vegetation burned. Fire emissions are injected homogeneously onto the boundary layer for this study. This parametrization can lead to uncertainties on the results as it impacts the transport of polluted plumes. The uncertainties concerning fire emissions are high, due to the accumulation of uncertainties on the emission factors, the area burned, the type of vegetation, etc. The uncertainty on the daily carbon emission is estimated at 100% (Turquety et al., 2014), and using dif-

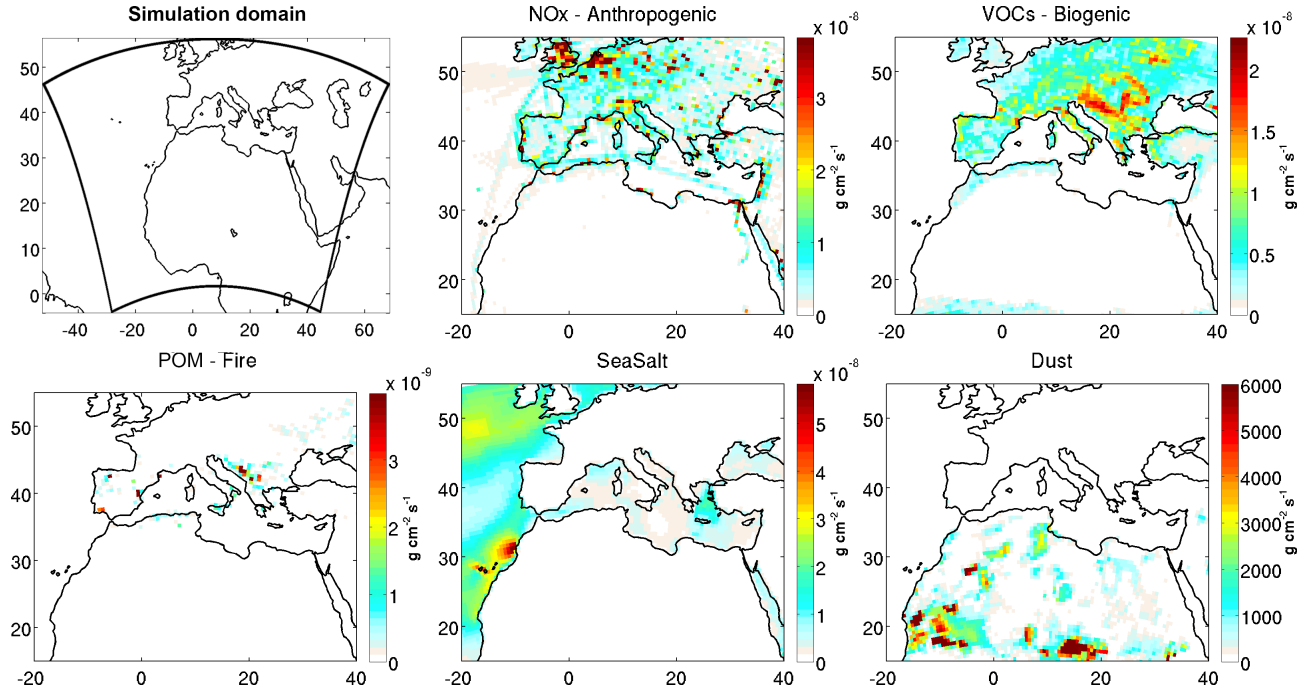

Fig. 5. *Total fluxes of different aerosol precursors or primary aerosol from each source during the summer of 2012: anthropogenic emissions of nitrogen oxydes (NOx), biogenic emissions of volatile organic compounds (VOCs), fire emissions of primary organic matter (POM), mineral dust and sea salt emissions.*

ferent inventories can lead to differences from -70% to 450% for outputs concentrations of CO (Daskalakis et al., 2014). The injection height can also be a source of uncertainty, as it can impact the transport pathway of a fire plume. Fires are the dominant source of primary organic matter, black carbon and other primary particulate matter in the MED-We (76, 34, and 58.6%, respectively) and MED-Ce (89.2, 46.4, and 69.9%, respectively) regions during the summer of 2012, where they occurred mainly in the Balkans and in the Iberian Peninsula (Figure 5). A smaller fraction of gaseous precursors are also emitted by fires (between 9 and 15% for NOx and NH_3 in MED-Ce). The distribution of primary organic matter fire emissions is shown in Figure 5. Regions affected by fires during this period are mostly located in the Balkans and in Spain (inducing the dominant emitted pollutants contributions in MED-We and MED-Ce).

The calculation of sea salt emissions is based on the Monahan (1986) scheme. Marine aerosols are produced from bubble bursting of whitecaps, generated by surface winds. Largest emissions occur over the Atlantic Ocean.

3.4 Sensitivity analysis

The CHIMERE CTM has been used to perform a number of sensitivity simulations, each with one source eliminated. The aim is to provide the approximate impact from the main regional source types~~(zone of influence, variability)~~. A complete budget would require the consideration of transport from boundary conditions as an additional source as well as the different sinks (wet and dry deposition, outflow). However, our main objective is to quantify the relative contribution from natural sources (dust, sea salts, fires, biogenic emissions of precursors) ~~since it is these emissions that can not~~ inside the regional domain, since these emissions cannot be controlled by regulations. Only these sources and anthropogenic sources are thus considered.

All the results will be presented in terms of difference between the reference simulation (all sources included) and the simulation in which the specific source is removed. For instance, to obtain the contribution of fire emissions on the concentration of a pollutant $[X]$, called $[X]_{fire}$, we computed:

$$[X]_{fire} = [X]_{ref} - [X]_{without\_fire\_emissions}$$

The acronym associated with the sensitivity simulations undertaken for the study are ANTH, BIOG, FIRE, DUST, and SALT for the baseline simulation minus the simulation without anthropogenic, biogenic, fire, mineral dust and sea salt emissions, respectively.

Note that the sum of all individual sources may not amount to the reference concentrations of PM due to ~~non-linarities~~ non-linearities in chemical processes. ~~Differences have been evaluated for the summer of 2012 to be , on~~ However, studies on particles sensitivities show that the main conclusions do not change with other methods such as source apportionment

or direct decoupled sensitivity, if the indirect effect is not significant (Koo et al., 2007, 2009; Burr et al., 2011).

In our study, the amount of $PM_{2.5}$ and PM_{10} formed by non-linear processes can be evaluated in the reference simulation. Therefore, the relative contribution from SOA and nitrates, which will be most impacted by non-linearities, to the total PM concentrations is calculated. On average over the domain ~~,~~ and for the reference simulation during the summer of 2012, 2.5% of total $PM_{2.5}$ is composed of SOA, and 1.3% of nitrates. Contributions to total $PM_{2.5}$ ~~for anthropogenic SOA , 2.3% for biogenic SOA and 4.8% for nitrates~~ from the sensitivity simulations have been evaluated to 1.3% and 1.1% of SOA and nitrates respectively from anthropogenic sources, and 1.5% and maximum 0.01% of SOA and nitrates from biogenic emissions. Contributions are 0.04% and 0.02% of SOA and nitrates respectively from fire sources.

4 Evaluation of model results

This section presents the results of the reference simulation (all emissions included), evaluated against the observations presented in section 2, to quantify the model performance for aerosol modelling.

4.1 Comparison with in situ PM surface concentrations

Surface PM simulation is evaluated using the correlation, the mean fractional error (MFE) and the mean fractional bias (MFB) between observations and collocated ~~modelled surface concentrations .~~ modeled surface concentrations :

$$MFB = \frac{1}{N}\sum_{i=1}^{N}\frac{(C_{mod}-C_{obs})}{(C_{mod}+C_{obs})/2} \quad (1)$$

$$MFE = \frac{1}{N}\sum_{i=1}^{N}\frac{|C_{mod}-C_{obs}|}{(C_{mod}+C_{obs})/2} \quad (2)$$

These statistical indicators are widely used in PM performance evaluation studies. Proposed by Boylan and Russell (2006) for PM, both the MFE and MFB must be lower than or equal to 50% and ±30% respectively to achieve the performance goals (level of accuracy considered to be close to the best a model can be expected to achieve), and must be lower than or equal to 75% and ±60% to meet the performance criteria (level of accuracy acceptable for standard ~~modelling~~ modeling applications). The MFB and MFE are computed at each station, and averaged. Additionally, the average of each absolute MFB is computed, the correlation coefficient (R), and the root mean square error (RMSE):

$$RMSE = \sqrt{\frac{\sum_{i=1}^{N}(C_{mod}-C_{obs})^2}{N}} \quad (3)$$

Tables 2 and 3 summarize the hourly and daily statistical results averaged over the regions NEU-We (~~393~~ 378 stations for PM_{10} and ~~133~~ 155 for $PM_{2.5}$), NEU-Ce (~~266 and 10)and~~ 280 and 95), MED-We (~~92 and 13). Other regions~~ 171 and 66), and MED-Ea (93 stations for PM_{10}). MED-Ce do not contain enough AirBase stations to allow statistically significant comparison (7 for PM_{10} and 1 for $PM_{2.5}$). For the time period and the entire domain of this study, the MFE and MFB on daily mean values are ~~42.9% and 21.6~~46.25% and 29.28% respectively for PM_{10}, and ~~44.3% and 31.8~~43.74% and 31.18% for $PM_{2.5}$. CHIMERE PM_{10} daily mean values meet thus the performance goal and $PM_{2.5}$ the performance criteria defined above. For hourly comparisons, the performance goal is not met on average over the region (MFE=~~52.8~~56.41% and MFB=~~20.4~~26.87% for PM_{10}, MFE=~~53.2~~55.05% and MFB=~~32.4~~30.99% for $PM_{2.5}$), but the model performance criteria is met. Indeed, the performance criteria is met for more than 90% of all the stations, and the performance goal is met for more than 40% of them.

In the regional comparisons, highest differences are obtained in the ~~MED-We region (82.6~~MED-Ea region (26.9% of the stations meet the performance criteria and only ~~16.3~~3.2% the performance goal for PM_{10}). A strong underestimation is noticed in this region with a MFB=-73.18%.

In the MED-We region, 82.5% of the stations meet the performance criteria and 25.7% the performance goal for PM_{10}. Peak concentrations are often overestimated by the model for both PM_{10} and $PM_{2.5}$, whereas levels are underestimated otherwise (MFB=~~-21.2% and -30.9~~-23.8% and -6.8% respectively for PM_{10} and $PM_{2.5}$).

The MFB is relatively good for other regions (in general under 20% except for NEU-We), indicating that PM concentrations do not have an excessive bias. The correlation coefficient is lower in the NEU-Ce region than in other regions except MED-Ea (0.38 for PM_{10} on ~~266~~ 280 stations) for hourly comparisons~~(~~, but not for daily averages with a correlation coefficient of 0.54~~)~~. This suggests an influence of local sources for which the diurnal profiles used for the simulations may not be ~~adapted to~~ appropriate for the region.

Figure 6 shows the temporal evolution of surface PM, averaged daily over the NEU-We, NEU-Ce and MED-We subregions, as well as MED-Ce and MED-Ea for PM_{10}. The levels of surface PM are consistent between observations and model, and the different peaks are well captured, especially in the northern part of the domain. In the Mediterranean Basin, levels are underestimated between the 4 and the 24 of July where no peak is detected neither by observations nor by the model. Peaks of pollution during the end of July and August are slightly overestimated. For PM_{10}, in ~~all three regions,~~ MED-We, NEU-We and NEU-Ce, a peak is overestimated by the model on 20 June by up to a factor of 4 (80 $\mu g\ m^{-3}$ instead of 20 $\mu g\ m^{-3}$ in MED-We). High values ~~(but lower) are~~ are also observed for this date on some of the Mediterranean stations such as Miramas (Fig-

ure 3) but not at other stations where the model overestimates strongly the peak value, particularly in the South of France. These peaks are attributed in section 5.1 to a dust transport event. However, there is no associated overestimation of AOD values by the model compared to the observations (MODIS or AERONET). This suggests that the ~~overstimation~~ overestimation in surface PM may be due to an overestimated transport at low altitudes, i.e. a wrong vertical distribution of the dust plumes. However, it may also be explained by an excess in total mass and a shift in the aerosol size distribution towards finer particles, as highlighted by Menut et al. (submitted) through comparisons of CHIMERE simulations with AERONET retrievals of the size distribution. An excessive PM concentration would then result in a correct AOD due to the variation of the extinction efficiency with the size of the aerosol.

4.2 Comparison with Aerosol Optical Depth (AOD) measurements

To evaluate modeled AOD, we compare it to two ~~dataset~~datasets: MODIS satellite data and AERONET data at specific stations. For each statistic, we collocate in time and space the simulated AOD with the corresponding dataset.

Figure 7 illustrates the time series of observed AOD and corresponding simulated values for each sub-region, and table 4 the associated statistics. The modelled AOD is close to the observations in all regions except for NEU-We, with a correlation coefficient ranging from ~~0.54~~ 0.56 (NEU-Ea) to ~~0.75~~ 0.77 (MED-Ce) and a MFE of ~~36.50~~34.3% for comparisons to AERONET and ~~24.63~~27.6% for comparisons to MODIS. The simulated AOD is ~~slightly~~ underestimated in the eastern and southern parts of the domain, ~~particularly compared to AERONET stations located in the eastern basin (MFB of -5.2~~with a MFB of -10% in MED-Ea ~~). Compared to MODIS, the simulated AOD has a moderate underestimation (MFB of -39.8% in MED-Ea~~for AERONET, -31.4% for MODIS. In MED-Ea, the evaluation with MODIS data is more robust as there is more information than AERONET data in this sub-region (Figure 1). This underestimation is also seen in the time series of Figure 7 ~~.~~ and coherent with the underestimation of PM_{10} noticed in the previous section. The variability of observations is greater than in the model, and than in other regions. The fine fraction of AOD from MODIS (not shown) is low, indicating that the total AOD in this region is due to coarse particles. The model is thus missing some coarse particles sources in this area.

Highest values are seen in MED-We, and the model manages to reproduce these values at the right timing (highest correlation coefficient) even if it moderately underestimates them (MFB of ~~-32.7~~-27.4% with respect to MODIS). Particularly, the peak at the beginning of July is underestimated by CHIMERE. The region with the lowest error and bias is MED-Ce, where the frequency and the intensity of peaks are lower.

5 Regional sensitivity to emission sources

In this section, the sensitivity of surface PM concentrations and total AOD to the different sources is analysed based on the series of sensitivity simulations described in section 3.4.

5.1 Surface particulate matter

Average relative contributions during the summer of 2012 to surface $PM_{2.5}$ and PM_{10} over the domain are presented in Figures 8 and 9. Table 5 summarizes the contributions in each sub-region of Table 1. As already highlighted in the general evaluation of the simulations, surface concentrations and total AOD are the largest over North Africa and the Mediterranean area, especially the Western Mediterranean area.

Table 5 shows that concentrations of PM_{10} are about three time higher than those of $PM_{2.5}$ (38.28μg m^{-3} versus 13 on average over the total period and domains). Surface PM_{10} also presents a stronger spatial variability (concentrations of surface PM_{10} ranges on average from 13.24 in NEU-Ea to 88.17μg m^{-3} in MED-We, whereas concentrations of surface $PM_{2.5}$ ranges from 9.46 in NEU-We to 15.66μg m^{-3} in MED-Ce).

The two most important contributors in the domain are anthropogenic and mineral dust emissions, which account, on average, respectively for 52% and 17% of surface $PM_{2.5}$, and 19% and 62% of surface PM_{10}. Anthropogenic emissions clearly dominate both surface $PM_{2.5}$ and PM_{10} in the northern part of the domain (up to 90% and 75% in average) but are also the main contribution to surface $PM_{2.5}$ above the Mediterranean Basin (~50%) and most particularly, as expected, around populated coastal areas.

Since the main dust emissions are located in North Africa, dust dominate the aerosol budget in this region. They also represent the main contribution to surface PM_{10} concentrations in the western Mediterranean area (Spain, South of France and Italy). The average contribution of mineral dust in the MED-We region is estimated to 86% for surface PM_{10} and 44% for $PM_{2.5}$. In this region, the mean concentration of surface PM_{10} over the period is exceeding the European threshold of 50 μg m^{-3} (88.17 μg m^{-3}). The contribution of mineral dust alone in this region is exceeding this threshold (75.63μg m^{-3}). Long-range transport also results in significant contributions in Northern Europe (22% of surface PM_{10} on average in region NEU-Ce).

Fire emissions are more sporadic and thus represent a lower contribution to the average surface concentrations. However, significant increase during the summer of 2012 is obtained in Spain and the Balkans, close to the main fire events (~~Cf.~~ Figure 5). The maps show an impact reaching up

Table 2. *Hourly performance statistics for the simulation of PM with CHIMERE (Mod.) compared to ~~AirBase~~ surface station measurements (Obs.) during the summer of 2012.*

Variable	Region	Number of stations	Mean (μg m^{-3}) Obs.	Mean (μg m^{-3}) Mod.	R	RMSE (μg m^{-3})	MFB (μg m^{-3})	|MFB|	MFE
PM_{10}	NEU-We	~~393~~ 378	16.05	16.70	~~17.07~~ 0.40	~~13.26~~ 12.54	~~-1.83~~1.24%	~~19.83~~18.20%	~~50.28~~49.41%
	NEU-Ce	~~266~~ 280	~~17.22~~ 17.84	~~16.13~~ 15.83	0.38	~~13.75~~ 13.32	~~-5.69~~-9.73%	~~17.45~~18.70%	~~52.99~~53.11%
	MED-We	~~92~~ 171	~~25.97~~ 23.31	~~25.20~~ 20.23	~~0.42~~ 0.47	~~27.86~~ 31.46	~~-21.16~~-23.76%	~~30.78~~29.64%	~~63.20~~59.88%
	MED-Ce	7	29.09	22.47	0.30	20.90	-23.45%	26.11%	55.15%
	MED-Ea	93	54.43	21.99	0.19	54.41	-73.18%	80.20%	89.44%
	ALL	~~760~~ 929	~~18.08~~ 21.86	~~17.93~~ 17.59	~~0.39~~ 0.38	~~15.38~~ 18.34	~~-5.34~~-14.14%	~~20.42~~26.87%	~~52.80~~56.41%
$PM_{2.5}$	NEU-We	~~133~~ 155	~~9.76~~ 9.38	~~11.73~~ 11.84	~~0.49~~ 0.51	~~8.20~~ 7.78	~~18.36~~22.97%	~~33.56~~34.47%	~~54.33~~54.82%
	NEU-Ce	~~10~~ 95	~~10.91~~ 11.64	~~11.74~~ 11.75	~~0.41~~ 0.40	~~6.61~~ 8.48	~~11.03~~12.10%	~~22.68~~21.61%	~~45.35~~53.40%
	MED-We	~~13~~ 66	~~14.46~~ 11.12	~~11.24~~ 9.83	~~0.37~~ 0.48	~~9.62~~ 8.71	~~-30.86~~-6.81%	~~33.59~~35.09%	~~56.06~~58.18%
	MED-Ce	1	24.68	22.69	0.57	10.22	-28.09%	28.09%	53.29%
	ALL	~~161~~ 317	~~10.44~~ 10.46	~~11.88~~ 11.40	~~0.48~~ 0.47	~~8.24~~ 8.14	~~13.36~~13.55%	~~32.35~~30.99%	~~53.18~~55.05%

Table 3. *Daily performance statistics for the simulation of PM with CHIMERE (Mod.) compared to ~~AirBase~~ station measurements (Obs.) during the summer of 2012.*

Variable	Region	Number of stations	Mean (μg m^{-3}) Obs.	Mean (μg m^{-3}) Mod.	R	RMSE (μg m^{-3})	MFB (μg m^{-3})	|MFB|	MFE
PM_{10}	NEU-We	~~393~~ 378	~~16.63~~ 16.04	~~17.04~~ 16.71	~~0.53~~ 0.56	~~10.45~~ 9.06	~~-3.38~~-1.15%	~~19.67~~17.60%	~~40.30~~36.31%
	NEU-Ce	~~266~~ 280	~~17.28~~ 17.84	~~16.16~~ 15.85	0.54	~~10.51~~ 9.82	~~-11.63~~-15.96%	~~20.40~~22.74%	~~41.46~~41.89%
	MED-We	~~92~~ 171	~~25.88~~ 23.27	~~25.28~~ 20.24	~~0.54~~ 0.62	~~22.83~~ 15.92	~~-23.55~~-28.53%	~~32.98~~33.41%	~~57.49~~51.21%
	MED-Ce	7	29.36	22.45	0.46	15.77	-30.59%	31.67%	46.68%
	MED-Ea	93	54.75	22.04	0.39	44.55	-79.60%	86.88%	90.24%
	ALL	~~760~~ 929	~~18.06~~ 21.89	~~17.92~~ 17.60	~~0.53~~ 0.54	~~12.16~~ 14.10	~~-8.52~~-18.73%	~~21.63~~29.28%	~~42.88~~46.25%
$PM_{2.5}$	NEU-We	~~133~~ 155	~~9.70~~ 9.33	~~11.67~~ 11.80	~~0.64~~ 0.65	~~6.33~~ 5.84	~~17.77~~22.27%	~~32.93~~33.57%	~~44.85~~44.39%
	NEU-Ce	~~10~~ 95	~~10.96~~ 11.61	~~11.88~~ 11.75	~~0.50~~ 0.55	~~5.31~~ 5.81	~~8.89~~4.71%	~~19.53~~22.47%	~~47.02~~39.10%
	MED-We	~~13~~ 66	~~14.39~~ 11.09	~~11.24~~ 9.79	~~0.57~~ 0.62	~~7.68~~ 6.72	~~-32.66~~-12.09%	~~35.92~~37.21%	~~51.57~~48.59%
	MED-Ce	1	24.58	22.64	0.67	16.03	-26.95%	26.95%	50.21%
	ALL	~~161~~ 317	~~10.41~~ 10.43	~~11.83~~ 11.37	~~0.62~~ 0.61	~~6.53~~ 6.01	~~12.54~~9.70%	~~31.79~~31.18%	~~44.32~~43.74%

to 20% locally on average during the summer. The largest regional contribution is obtained for the MED-Ce region, with 12% of $PM_{2.5}$ associated with fires.

As expected, sea salt emissions are the main contribution to PM above the Atlantic Ocean. However, their relative contribution above continents is low, except in the coastal areas and over North-Western Europe where is reaches 29% of surface PM_{10}. Over coastal cities, the impact of sea salts at the surface can be as large as that of anthropogenic emissions. Biogenic emissions have an important contribution to PM in Central Europe, where they are mainly located (figure 5). They account for almost 20% of surface $PM_{2.5}$ in the NEU-Ce region.

Figure 11 shows the temporal evolution of surface $PM_{2.5}$ and PM_{10}, and their associated source contributions, over the different sub-regions depicted in Table 1: NEU-We, NEU-Ce and NEU-Ea, MED-We, MED-Ce and MED-Ea. It shows that the daily variability above the chosen regions is large, especially for surface PM_{10}, with diverse contributions. The variability in the Northern part of the domain is mainly controlled by anthropogenic emissions. However, the NEU-We region is also frequently affected by mineral dust (20-21 June, 1 July, end of August) and by sea salts for surface PM_{10} concentrations. In the NEU-Ce and NEU-Ea regions, most of the large peaks in PM_{10} are attributed to mineral dust transport events.

Extreme concentrations are simulated in the Western and Central Mediterranean areas (MED-We and Ce), here again mainly due to large contributions from mineral dust emissions. These impact mainly surface PM_{10}, while $PM_{2.5}$ are often dominated by a more constant contribution from anthropogenic emissions. Fires are another significant contribution in these regions at the end of July and August for surface $PM_{2.5}$.

Comparisons to ~~AirBase~~ surface observations highlighted an overestimate of the largest PM_{10} peaks in the simulations

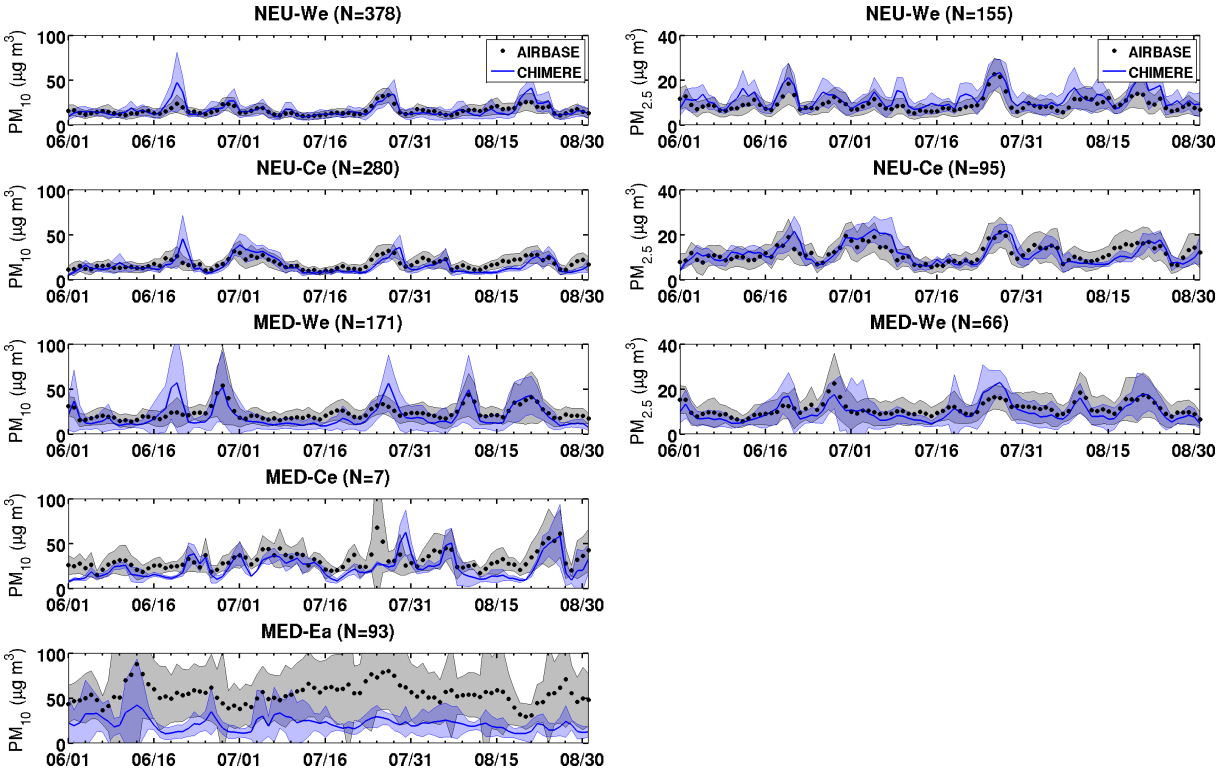

Fig. 6. *Temporal evolution during the ~~Summer~~ summer of 2012 of observed daily mean surface PM_{10} (left column) and surface $PM_{2.5}$ (right column) concentrations at AirBase stations with the two more ChArMeX rural stations in Corsica (number in each region indicated by the value of N), in addition to corresponding and collocated simulated daily mean surface concentration from CHIMERE (blue line). The corresponding standard deviation is indicated in filled area.*

Table 4. *Hourly performance statistics of AOD simulated by CHIMERE (Mod.) during the summer of 2012, together with the observed AOD from AERONET at 500 nm and MODIS at 550 nm (Obs.).*

Variable	Region	Number of stations	Number of pairs	Mean Obs.	Mean Mod.	R	RMSE	MFB	MF
AOD AERONET (500 nm)	NEU-We	17	~~733~~ 748	~~0.16~~ 0.15	0.15	~~0.44~~ 0.49	~~0.11~~ 0.10	~~-1.56~~-1.63%	~~42.954~~0
	NEU-Ce	5	~~322~~ 326	~~0.23~~ 0.22	0.19	~~0.70~~ 0.71	0.10	~~-14.13~~-15.22%	~~35.173~~4
	NEU-Ea	6	~~240~~ 245	0.19	0.17	~~0.64~~ 0.72	~~0.08~~ 0.07	~~-11.41~~-14.53%	~~30.042~~9
	MED-We	25	~~1694~~ 1729	~~0.19~~ 0.20	0.17	~~0.73~~ 0.77	~~0.10~~ 0.09	~~-3.52~~-6.46%	~~37.473~~4
	MED-Ce	7	~~418~~ 427	0.22	0.21	~~0.70~~ 0.69	0.08	~~0.53~~-1.59%	~~29.932~~7
	MED-Ea	5	~~438~~ 448	0.21	~~0.19~~ 0.18	~~0.65~~ 0.71	~~0.08~~ 0.07	~~-5.17~~-9.96%	~~27.952~~4
	ALL	65	~~3845~~ 3923	0.19	0.17	~~0.64~~ 0.68	~~0.10~~ 0.09	~~-4.24~~-6.36%	~~36.503~~4
AOD MODIS (550 nm)	NEU-We		225	0.19	~~0.14~~ 0.13	~~0.35~~ 0.37	~~0.07~~ 0.08	~~-29.64~~-27.40%	~~36.792~~9
	NEU-Ce		58	0.21	~~0.17~~ 0.16	0.70	0.07	~~-24.91~~-15.08%	~~31.662~~2
	NEU-Ea		184	0.18	~~0.17~~ 0.16	~~0.54~~ 0.56	0.06	-8.31%	~~26.801~~3
	MED-We		537	0.30	0.22	~~0.73~~ 0.74	0.10	~~-32.66~~-27.39%	~~33.213~~1
	MED-Ce		449	0.22	0.19	~~0.75~~ 0.74	0.04	~~-12.60~~-6.10%	~~17.712~~2
	MED-Ea		327	0.25	~~0.17~~ 0.16	0.67	0.10	~~-39.84~~-31.35%	~~39.843~~8
	ALL		3380	0.24	~~0.19~~ 0.18	~~0.62~~ 0.63	0.06	~~-24.60~~-18.75%	~~24.632~~7

in the NEU-We, NEU-Ce and MED-We regions (Figure 11). 790 too large in the model.
This suggests that mineral dust transport at low altitudes is

Table 5. *Contributions of each emissions source on surface $PM_{2.5}$ and PM_{10} concentrations and AOD for the full domain and the different sub-regions indicated in Table 1 over the period (1 June to 31 August 2012).*

Region	Source	Surface $PM_{2.5}$		Surface PM_{10}		AOD	
		$\mu g\ m^{-3}$	%	$\mu g\ m^{-3}$	%	ad.	%
All domain	All sources	13.00		38.28		0.19	
	Anthropogenic	6.76	52.01%	7.10	18.56%	0.07	33.95%
	Fires	0.82	6.27%	0.92	2.39%	0.01	5.46%
	Dust	2.17	16.67%	23.87	62.35%	0.05	23.26%
	Biogenic	1.41	10.83%	1.43	3.75%	0.03	14.04%
	Sea Salt	0.59	4.53%	2.73	7.12%	0.0012	0.59%
NEU-We	All sources	9.46		15.10		0.18	
	Anthropogenic	7.11	75.13%	7.44	49.28%	0.10	54.87 %
	Fires	0.12	1.22 %	0.13	0.86 %	0.00	2.20%
	Dust	0.15	1.62 %	1.18	7.84%	0.01	4.83%
	Biogenic	0.68	7.24%	0.69	4.57%	0.01	5.01%
	Sea Salts	0.68	7.19%	4.33	28.70%	0.00	1.14%
NEU-Ce	All sources	11.36		15.86		0.20	
	Anthropogenic	7.16	62.98%	7.56	47.67 %	0.09	42.65%
	Fires	0.42	3.66 %	0.45	2.82%	0.01	4.62 %
	Dust	0.52	4.58%	3.45	21.78%	0.02	9.97 %
	Biogenic	2.48	21.83 %	2.51	15.82%	0.04	21.51 %
	Sea Salts	0.16	1.42%	0.58	3.68%	0.00	0.43 %
NEU-Ea	All sources	9.78		13.24		0.19	
	Anthropogenic	4.91	50.14%	5.30	40.00%	0.06	33.99%
	Fires	0.72	7.31%	0.75	5.64%	0.01	7.26%
	Dust	0.35	3.57%	2.28	17.19%	0.02	7.95%
	Biogenic	1.51	15.45%	1.53	11.57%	0.04	22.01%
	Sea Salts	0.12	1.27%	0.43	3.27%	0.00	0.26 %
MED-We	All sources	15.15		88.17		0.23	
	Anthropogenic	4.92	32.50%	5.17	5.86%	0.04	18.72%
	Fires	0.83	5.45%	0.95	1.08%	0.01	4.51 %
	Dust	6.54	43.19 %	75.63	85.78 %	0.11	49.20 %
	Biogenic	0.82	5.38%	0.84	0.95 %	0.02	7.12 %
	Sea Salts	0.62	4.12 %	2.96	3.36%	0.00	0.58 %
MED-Ce	All sources	15.66		33.22		0.20	
	Anthropogenic	8.54	54.55%	8.89	26.77 %	0.06	31.50%
	Fires	1.91	12.22%	2.16	6.51%	0.02	9.82 %
	Dust	1.36	8.66%	14.39	43.31 %	0.04	22.64 %
	Biogenic	1.84	11.77 %	1.90	5.70 %	0.03	16.75%
	Sea Salts	0.90	5.75 %	3.60	10.83 %	0.00	0.57%
MED-Ea	All sources	12.90		22.90		0.17	
	Anthropogenic	7.83	60.67%	8.24	35.98%	0.07	41.01 %
	Fires	0.45	3.48%	0.50	2.20%	0.01	3.81%
	Dust	0.78	6.06%	7.09	30.98%	0.02	10.88%
	Biogenic	1.42	11.02%	1.45	6.34%	0.03	18.64%
	Sea Salts	0.67	5.17%	2.84	12.40%	0.00	0.46%

5.2 Vertical distributions and AOD

Figure 12 presents the vertical distributions of PM in the simulations, averaged over each of the sub-regions. As already highlighted in the discussion above, surface concentrations are strongly affected by anthropogenic emissions, except in the western and central Mediterranean Basins, which are dominantly affected by mineral dust transport. ~~In this area,~~ The vertical structures of the simulated dust layers have

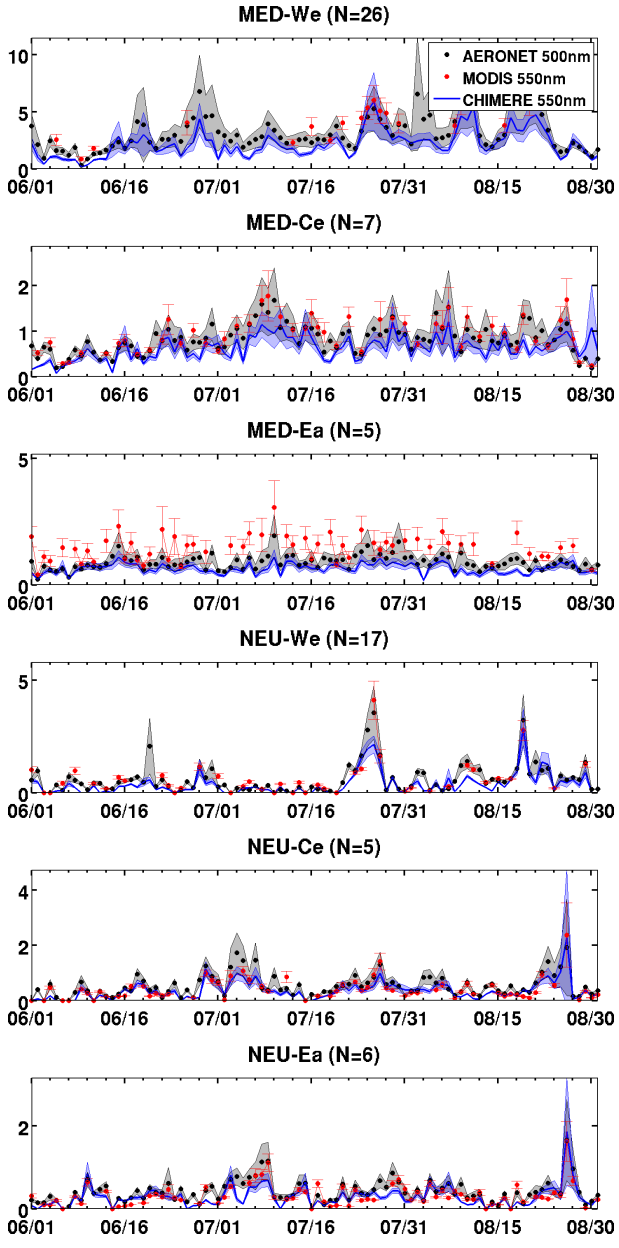

Fig. 7. *Temporal evolution of the daily mean AOD observed at 500 nm at the AERONET stations (black dots) and at 550 nm from MODIS Aerosol Products (red dots), in addition to simulated AOD at 550 nm by the CHIMERE model (blue line) during the ~~Summer~~ summer of 2012. The standard deviation among the stations is indicated in grey and blue area for AERONET and CHIMERE, and with red bars for MODIS. Number of stations in each region is indicated by the value of N.*

been evaluated in Vuolo et al. (2009) with CALIOP LIDAR profiles during June to September 2006 and January to March 2007. It has been shown that the model has a vertical overspread of 50% in summer compared to the observations, but less multilayers dust situations. However, in MED-We and MED-Ce, the vertical contribution from dust range from the surface to about 4-5 km (Figure 12), which is an usual pattern compared to the climatology of Nabat et al. (2013). Dust affects mainly the free troposphere over the northern regions.

Fires and biogenic emissions are also important contributions, particularly for $PM_{2.5}$. They often have maximum contributions in the lower troposphere. Sea salts contribute to PM_{10} in Western Europe and the Mediterranean region, as well as in the central Mediterranean region, but are confined to the lower-most troposphere.

Contributions to the total AOD, which includes the signature of aerosols over the full vertical column, follow the same general patterns as the contributions to surface PM_{10} discussed above (average relative contributions in Figure 10 and Table 5). However, the contribution of sea salts remains very low (<1%)~~, due to a low radiative impact but also to the fact that sea salts remain close to the surface and make thus a low contribution to the full vertical column load~~.

Temporal variability over the selected sub-regions (Figure 11, third column) shows that, similarly to what was obtained for surface PM, anthropogenic emissions control the variability in the NEU-We region, while mineral dust emissions are the main contribution in the MED-We region. The fire episodes of the end of August also contribute significantly to the total AOD in the NEU-Ea and MED-Ce regions. Compared to the total column (vertically integrated) concentrations of PM ~~, contributions from fine particles to AOD are larger. This is due to the fact that~~ (not shown), source contributions to AOD follow contributions to $PM_{2.5}$ concentrations. At the considered wavelength (500 nm), fine particles from anthropogenic or local fire emissions, even concentrated in the first layers, ~~are more active optically~~ contribute more significantly (34% for mean anthropogenic contribution) than larger mineral dust particles (23%) at the considered wavelength (500 nm) ~~, and hence contribute more significantly~~ to the calculated AOD.

6 Contributions to air quality threshold exceedances

The European Union has developed legislations to establish health based standards for a number of atmospheric pollutants. For PM_{10}, the ~~limit is~~ air quality limit value is set, for health based considerations, to a daily mean of 50 μg m^{-3} and an annual mean of 40 μg m^{-3}. For $PM_{2.5}$, there is no regulation in Europe except for a quality aim of 25 μg m^{-3} in annual mean. In this section, the exceedances of the daily mean limit for PM_{10} concentrations are ~~analysed.~~ analyzed. We also analyze $PM_{2.5}$ exceedances of a limit of 25 μg m^{-3} per 24h (World Health Organisation recommendations). The number of stations in daily exceedances are calculated for both ~~AirBase~~ observations and collocated CHIMERE simulations. The simulations were undertaken at a regional scale,

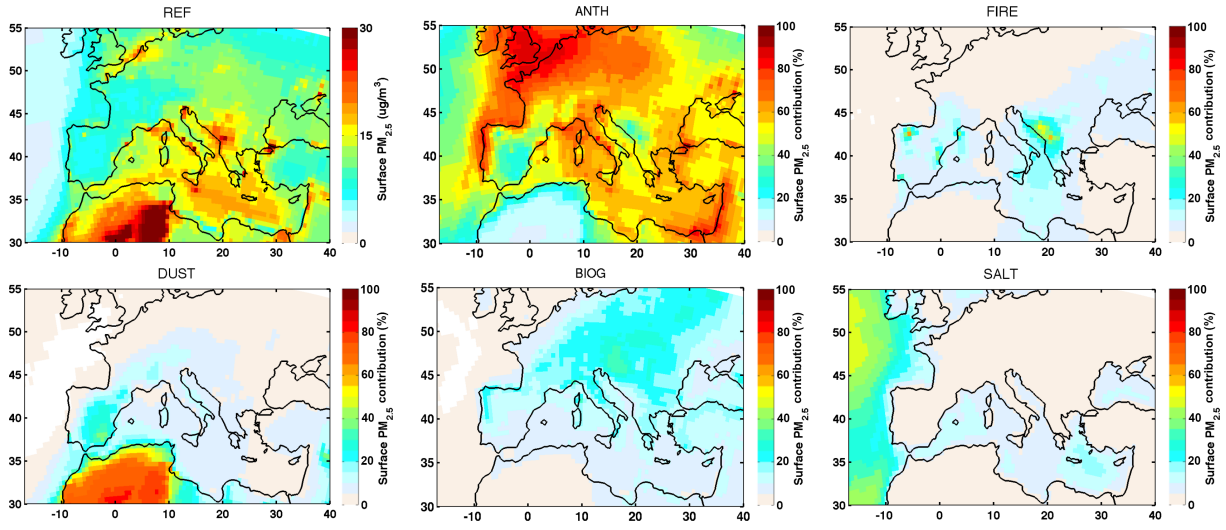

Fig. 8. *Relative contribution of each source (i.e. the baseline simulation minus the sensitivity simulation where the respective source has been eliminated) to the simulated surface $PM_{2.5}$, averaged over the period (1 June to 31 August 2012). The first plot represents the reference surface concentration over the same period.*

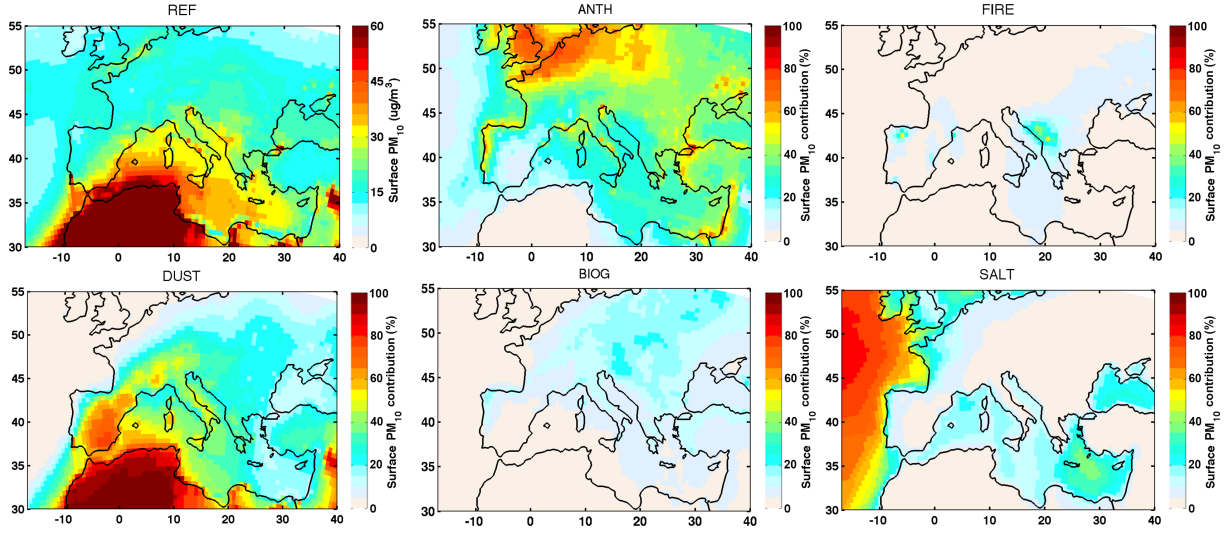

Fig. 9. *Relative contribution of each source (i.e. the baseline simulation minus the sensitivity simulation where the respective source has been eliminated) to the simulated surface PM_{10}, averaged over the period (1 June to 31 August 2012). The first plot represents the reference surface concentration over the same period.*

so that only exceedances at rural and background sites are considered.

In total, 96.2% of the PM_{10} daily means are under the threshold of 50 μg m^{-3} in both observations and co-located simulation. The analysis will focus on the 3.8% other cases. Figure 13 presents the number of stations where the daily mean ~~concentration~~ concentrations of PM_{10} ~~is~~ and $PM_{2.5}$ are above 50 μg m^{-3} and 25 μg m^{-3} respectively, in the observations or the model simulations within each sub-region (only the sub-regions where there are ~~AirBase~~ stations to compare with).

It clearly shows that the model detects more exceedances than the observations in MED-We, NEU-We and NEU-Ce (in total ~~1965 versus 624~~ 1964 versus 881 in the observations for PM_{10}, positive bias ~~from 54.5, 82.2 and 72.2% for respectivelyMED-We, NEU-We and NEU-Ce~~of 42.5%, 86.6% and 64.7% respectively), and sometimes not at the same time (correlation coefficient of respec-

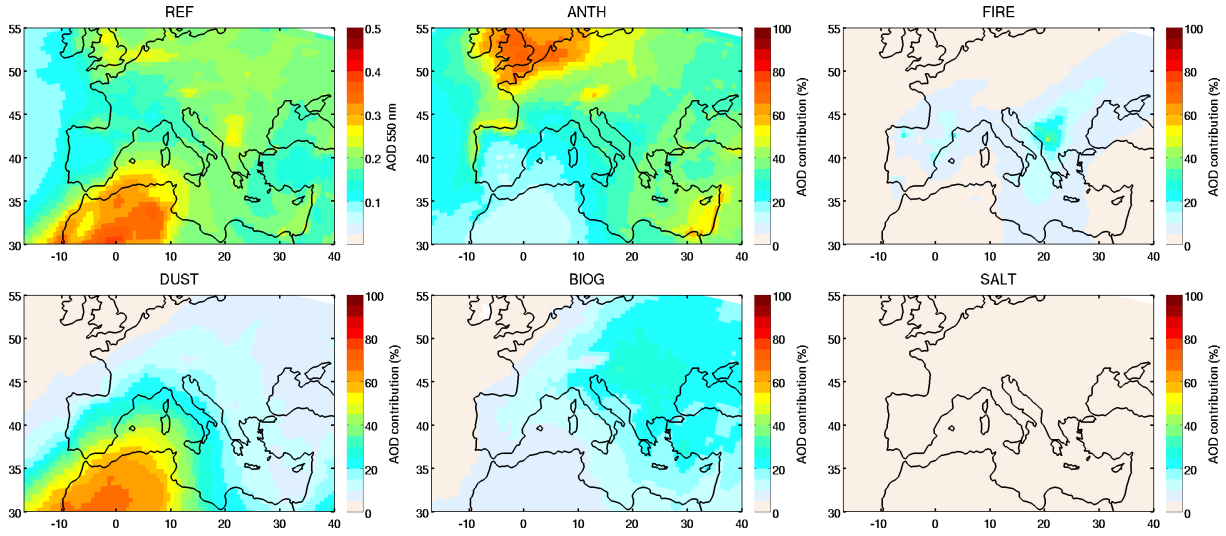

Fig. 10. *Relative contribution of each source (i.e. the baseline simulation minus the sensitivity simulation where the respective source has been eliminated) to the simulated AOD at 550 nm, averaged over the period (1 June to 31 August 2012). The first plot represents the reference simulation of AOD over the same period.*

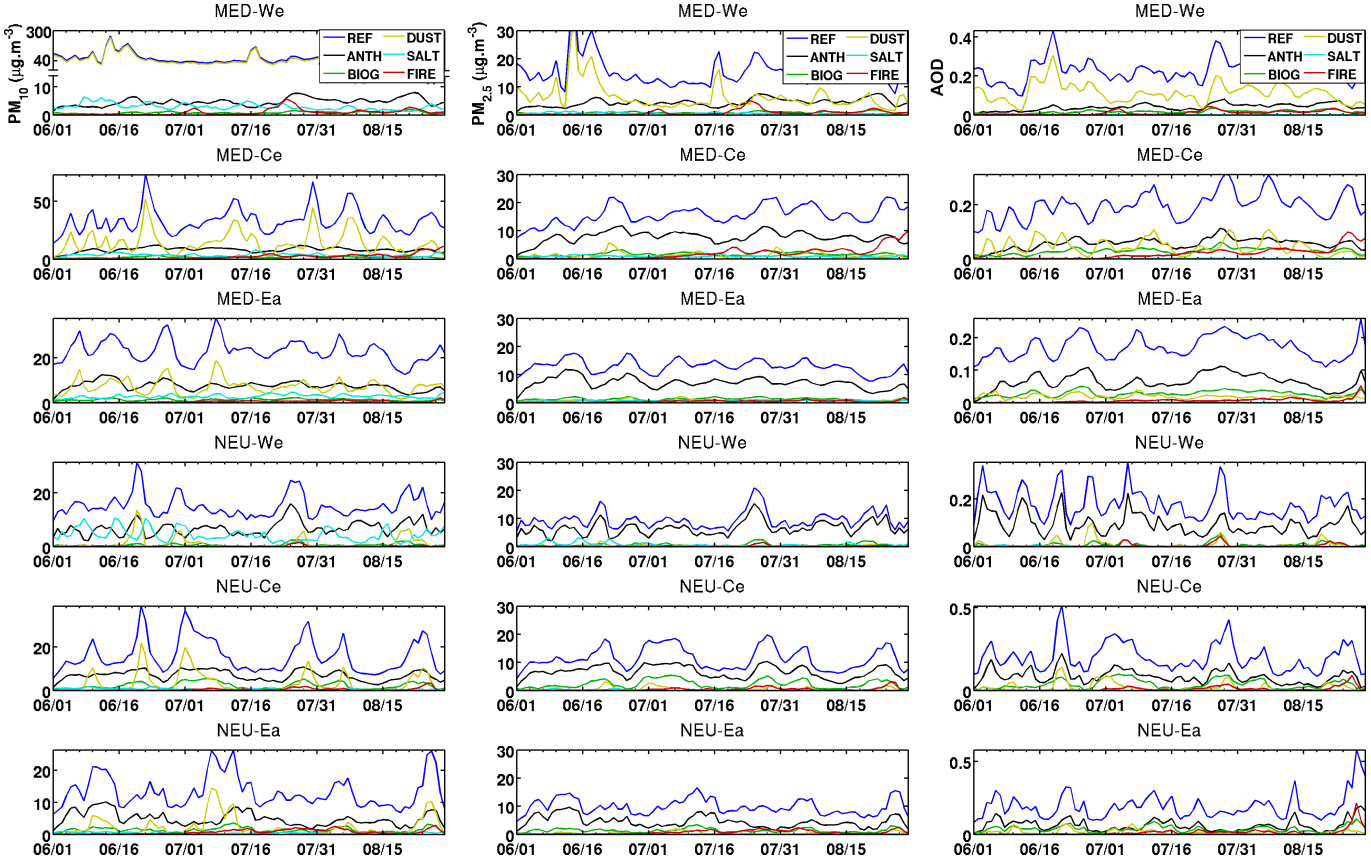

Fig. 11. *Temporal evolution during the ~~Summer~~ summer of 2012 (1 June to 31 August 2012) of the total simulated surface PM_{10} ~~(left column)~~ and surface $PM_{2.5}$ ~~(right column)~~ concentrations, and AOD, with the contributions from each source (i.e. the baseline simulation minus the sensitivity simulation where the respective source has been eliminated), averaged within each sub-region indicated in Table 1.*

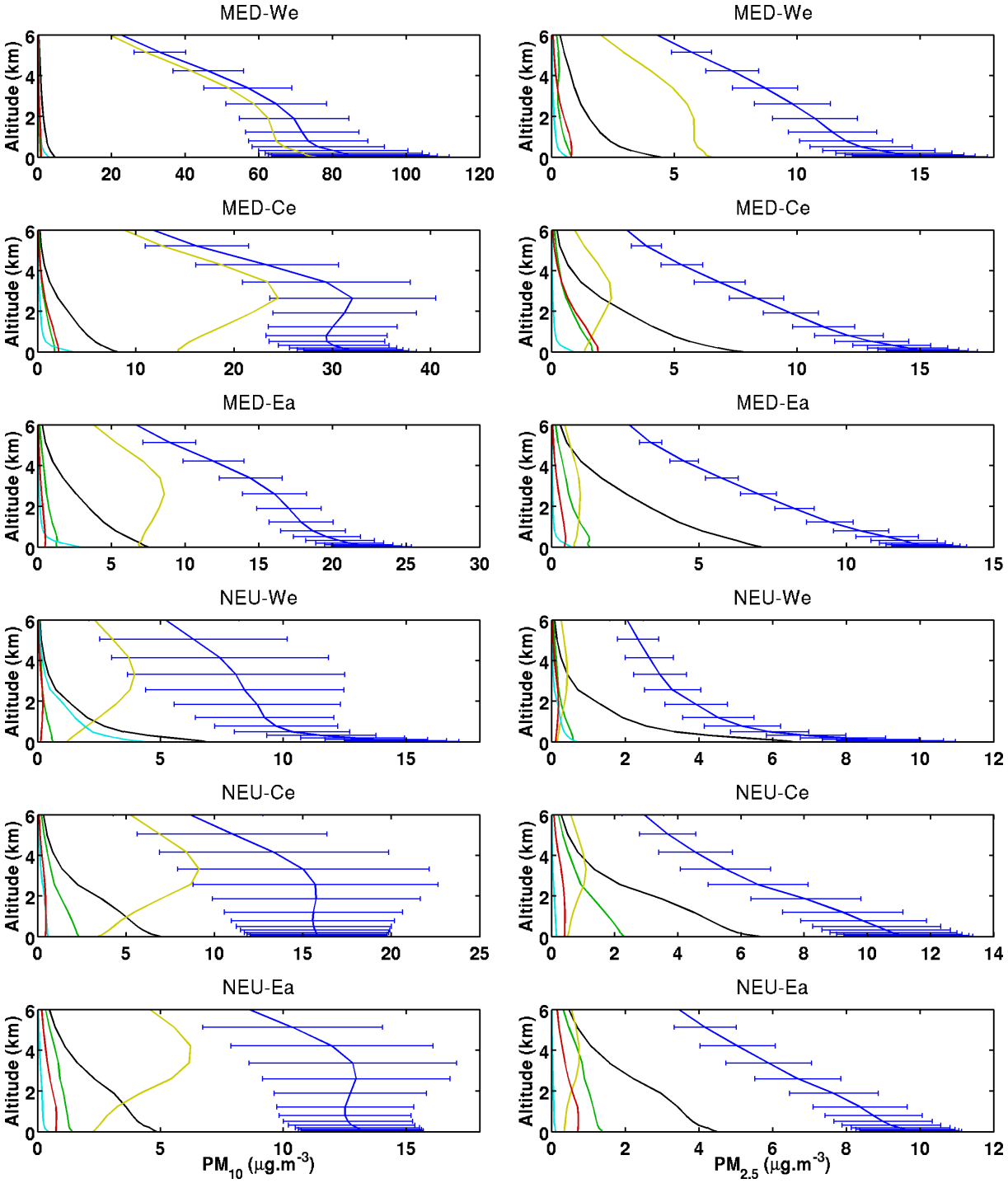

Fig. 12. *Mean vertical profiles of PM_{10} (left column) and $PM_{2.5}$ (right column) for each sub-region indicated in Table 1 and for each contributions. The standard deviation is represented only for the reference simulation by the horizontal bars.*

tively ~~0.6, 0.48 and 0.4). 43.6%of the 624~~ 0.68, 0.42 and 0.43). In the MED-Ea region, several exceedances, particularly in the observations, are not reproduced in the model (MFB=-73.18%). The model only sees exceedances from anthropogenic emissions (80% of the cases). The global underestimation of PM_{10} certainly due to missing coarse particles sources described in section 4.1 does not allow the analysis of exceedances in this region.

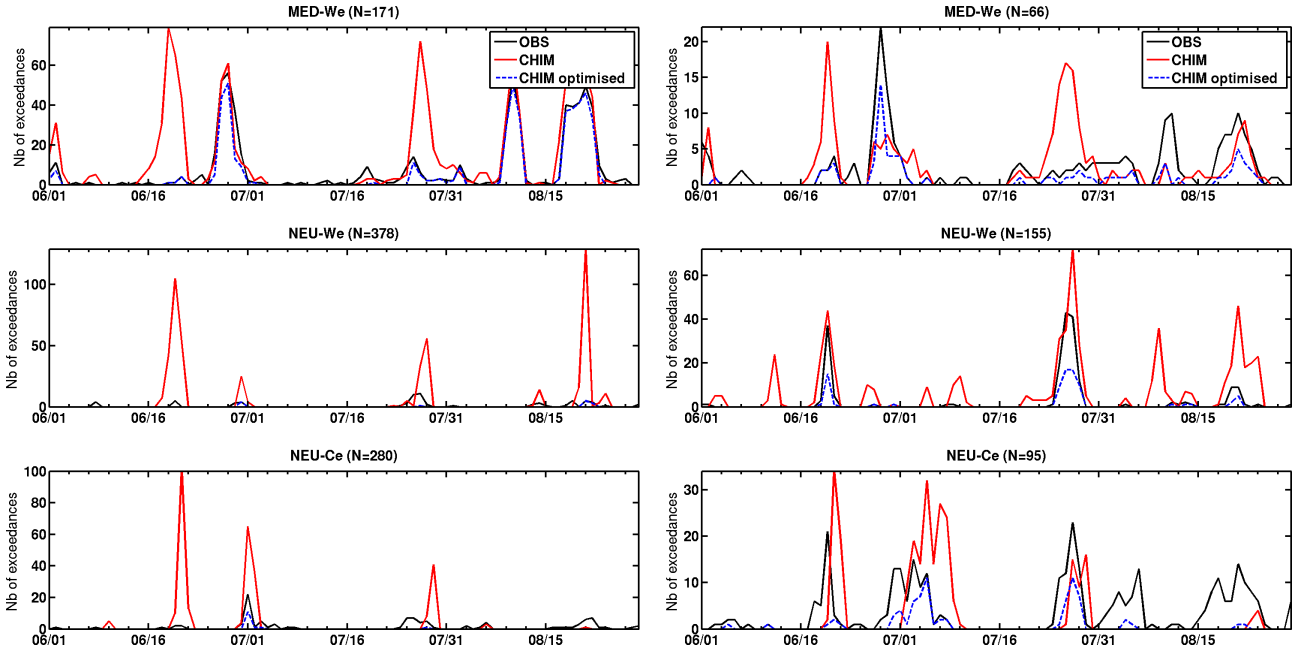

Fig. 13. *Number of stations in daily exceedances of the European Union air quality threshold of 50 $\mu g\ m^{-3}$ for daily mean PM_{10} concentrations (left panel), and in daily exceedances of the WHO recommendation of 25 $\mu g\ m^{-3}$ for $PM_{2.5}$ concentrations (right panel). This time series is computed during the ~~Summer~~ summer of 2012 (1 June to 31 August 2012), as observed at the rural and background ~~AirBase~~ stations (black line) and simulated by the CHIMERE model at the same locations (red line). The ~~red~~ dashed blue line ~~corresponds to~~ is the ~~simulated~~ number of ~~stations in daily~~ exceedances when the ~~threshold~~ bias is ~~set to respectively 75, 58 and 62 $\mu g\ m^{-3}$~~ removed for ~~MED-We~~each point, ~~NEU-We and NEU-Ce, when the contribution of mineral dust is more than 60% of the total concentration~~as described in Section 6.*

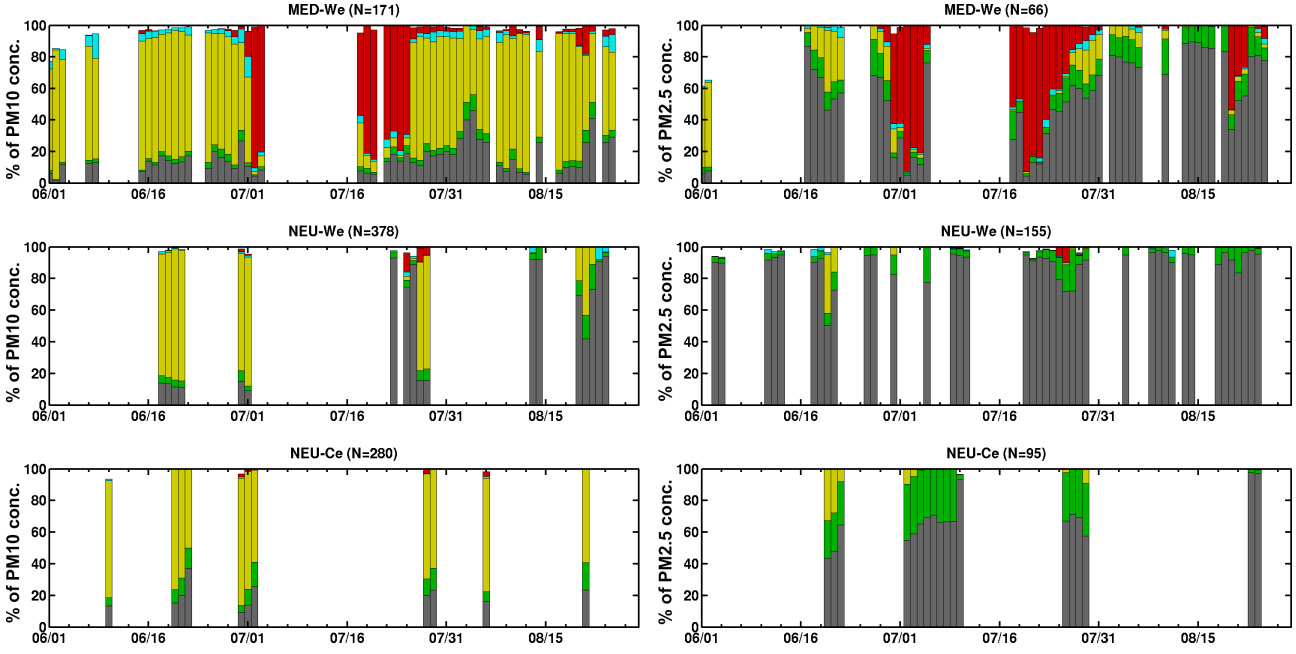

Fig. 14. *Simulated relative contribution of each source to surface PM_{10} ~~concentration~~ and $PM_{2.5}$ concentrations during the ~~Summer~~ summer of 2012 (1 June to 31 August 2012), on average when exceedances of the daily air quality threshold are detected only by ~~both observations and~~ the model at the ~~same time and location~~stations (N is the number of stations in each region).*

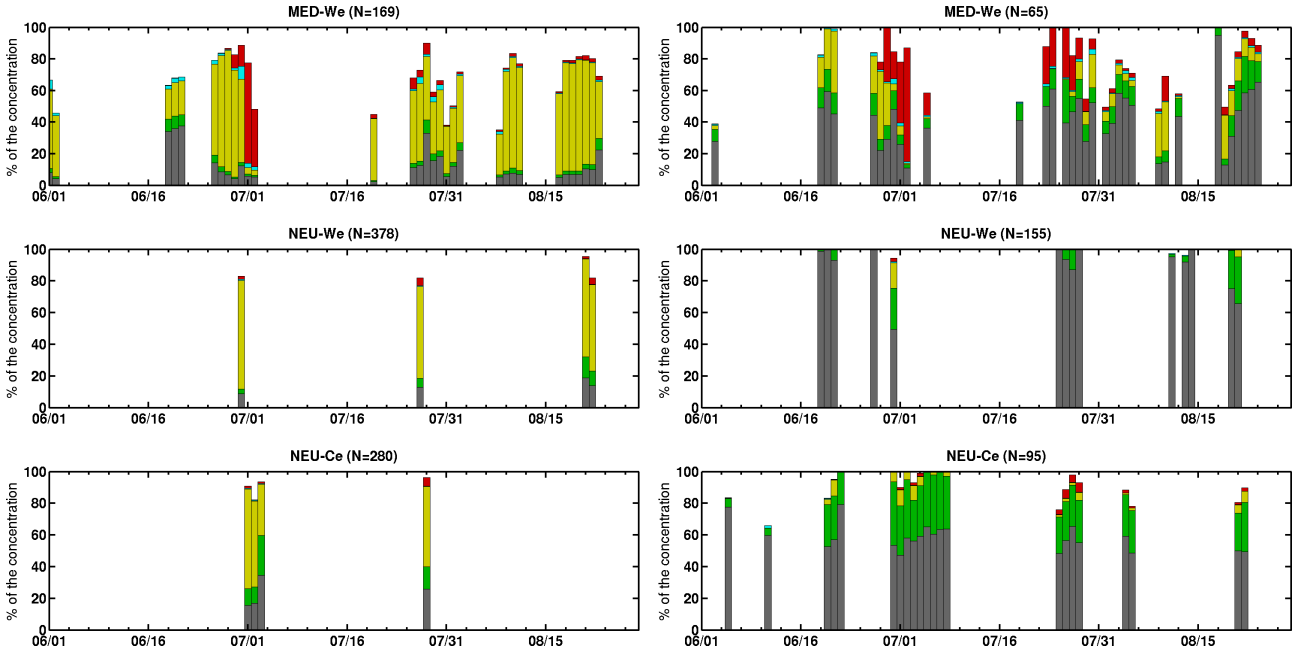

Fig. 15. *Simulated relative contribution of each source to surface PM_{10} and $PM_{2.5}$ concentrations during the summer of 2012 (1 June to 31 August 2012), on average when exceedances of the daily air quality threshold are detected by both observations and ("optimized") model at the same time and location. Results are shown for regions where stations are available (N is the number of stations in each region). The model for this figure is "optimized" at each point of each station to avoid excessive attributions (see section 6).*

For PM_{10}, 52.7% of the 881 observed exceedances are correctly captured by the model, the majority of them located in MED-We. More particularly, the event of 27-28 June is well simulated (~~Cf.~~ Figure 3) and is correctly detected in terms of number of stations in daily exceedances (29 exceedances for observations, 35 for the model, among the 92 stations). This is also the case for the two peaks in August (around 20-30 exceedances). For $PM_{2.5}$, only 23.5% of exceedances are correctly simulated, with the majority in NEU-We.

Figure ~~15~~ 14 shows the contribution of each source when ~~the concentration exceeds the threshold for both model and observations. For these peaks, the contribution of mineral dust is predominant, mixed with anthropogenic pollution and fires from 28 June to 3 July (fires alone contribute to 3 exceedances at that time), as well as biogenic emissions from 18 to 23 August.~~

an exceedance is detected only by CHIMERE, and not in the observations. The peak of the 20-21 June is present in the model simulations at almost every ~~AirBase stations , but only at some stations in the observations (see section 4.1). The~~ stations so that the number of simulated exceedances is ~~thus~~ a lot larger than in the ~~AirBase dataset. This~~ observational dataset. The model only exceedances associated with this peak is attributed to ~~a mineral dust event that is overestimated by the model in most of the stations, with a high contribution in MED-We, and a lower contribution in other~~ mineral dust in the three regions (mixed with anthropogenic and biogenic contributions).

~~Exceedances are also detected at the end of July, between 27 and 31, in the three sub-regions. The model here again overestimates~~ The model overestimates also the number of stations in daily exceedances at the end of July (37 versus 6 for observations in MED-We, 82 versus 14 for NEU-We ~~). The sensitivity simulations indicate that the concentration of PMwas high due to contributions from all the different sources: mineral dustmainly, anthropogenic~~ for PM_{10}), with contributions from mineral dust, anthropogenic sources, and fires (stronger in MED-We and NEU-Ce)~~associated to biogenic in NEU-We and NEU-Ce~~.

~~In MED-We, 240 exceedances are seen~~ Among the 464 PM_{10} exceedances detected by both the model and the observations~~. Without the anthropogenic sources, there are still 222 exceedances, so that 92.5% of them~~ , 76.7% are due exclusively to dust, and 1.7% to fires. The other 100 exceedances are due to ~~natural sources according to CHIMERE. In NEU-We, on the 17 exceedances detected by both the~~ a mix contribution of dust (from 78.1% in MED-We to 85% in NEU-We), anthropogenic sources (about 15% in the three regions), biogenic sources (from 5.5% in MED-We to 11.2% in NEU-Ce) and fires (from 1.7% in NEU-Ce to 10.2% in MED-We). For $PM_{2.5}$, 176 on 1063 detections are coherent between the model and the observations, ~~35.3%~~ and 33.5% and 7.3% are due exclusively to anthropogenic and fires sources respectively. The other 104 exceedances are due

to natural sources . Finally in a mix between anthropogenic sources (from 64.2% in MED-We to 92.1% in NEU-We), biogenic sources (from 14.4% in NEU-We to 39.3% in NEU-Ce, 75% of the 13 coherent exceedances are due), fires (from 1% in NEU-We to natural sources 15.6% in MED-We) and dust (1.7% in NEU-We to 17.5% in MED-We).

Using a linear regression on modelled versus observed PM_{10} concentrations when the contribution of mineral dust is more than 60%, the model values corresponding to the 50 These source contributions on daily exceedances might be uncertain due to the high overestimation of the model. An optimization is proposed to estimate more robust contributions of observed exceedances.

First, the bias on background levels is evaluated at each measurement station. The background is defined as the baseline concentration, on days when no significant peak is measured. It is generally associated with anthropogenic and biogenic sources, which have relatively low variability during the summer compared to dust and fire emissions.

The average "background bias" is estimated to -6.3 μg m^{-3} limit in the observations are found to be 75, 58 and 62 for PM_{10} and -1.9 μg m^{-3} for $PM_{2.5}$ in MED-We, -0.93 μg m^{-3} and 1.3 μg m^{-3} in NEU-We, and -3.2 μg m^{-3} and -0.2 μg m^{-3} in NEU-Ce, respectively. Setting higher daily limits values for the model (in the detection of an exceedance) only for dust events could result in better agreement between modelled and observed number of stations in daily exceendance. The corresponding comparisons are shown in Figure 13 (dashed red line). This method allows a slight reduction of the biases (from 54.5% on average over all stations.

Then for sporadic sources, i.e. for the dust and fires, the resulting bias at each point of a peak is subtracted only for contribution concentrations of the corresponding source. This processing is applied only when the model overestimates the concentrations with respect to observations, but not when a peak is detected only by the observations.

The corresponding new number of exceedances with this calculation is shown on Figure 13 in dashed blue line. The total number of exceedances is then 549 and 256 respectively for PM_{10} and PM2.5 (instead of 1964 and 1063 initially) in total for the three regions, all of them detected also in the observations.

For these "optimised" concentrations, Figure 15 shows the contribution of each source to the simulated exceedances. For the peaks at the end of June, the contribution of mineral dust to the exceedances is predominant particularly for PM_{10}, mixed with anthropogenic pollution and fires from 28 June to 3 July (fires alone contribute to 3 exceedances at that time), as well as biogenic emissions from 18 to 34.5% for 23 August. In total, the only sources that result exclusively (i.e. when their contribution alone on PM concentration is more than the threshold of 50 μg m^{-3}) in an exceedance are dust (in 35.9% of the cases, i.e. 197 exceedances on the 549 observed and simulated) and fires (in 0.7% of the cases, i.e. 4 exceedances). The other 348 exceedances are due to a mixed contribution of several sources: anthropogenic sources contribute from 14.9% (NEU-We) to 24.2% (NEU-Ce) of the concentrations, biogenic from 4.1% (MED-We, from 82.2% to 74.9% for NEU-We, and from 72.2% to 48.6% for NEU-Ce). However, large discrepancies remain on some events, showing that this does not resolve the modelled excessive spatial spread and intensity of some mineral dust events.

This analysis shows that air quality levels remain difficult to diagnose for this regional simulation. Exceedances due to mineral dust are well captured by the model in the sub-region closest to the mineral dust outflow () to 15.7% (NEU-Ce), fires from 2.2% (NEU-Ce) to 7.2% (MED-We), except for the event of 20-21 July. In other sub-regions, CHIMERE overestimates pollution levels attributed to mineral dust above many stations, indicating that plumes are either simulated at too low altitudes, either too spread over the region. Fires also represent a large sourceof uncertainty for the peak around the), and dust from 49.5% (MED-We) to 67% (NEU-We).

For $PM_{2.5}$ exceedances, the only sources that result exclusively in concentrations above 25 July in MED-We. In other regions, the mix between mineral dust, anthropogenic and biogenic sources leads to exceedances in the model not systematically seen at the stations and vice versa. Even if natural sources as mineral dust events are particularly difficult to estimate, their contribution μg m^{-3} are anthropogenic sources (54 exceedances on the 256 observed and simulated at the same time, i.e. 21.1%) and fires (5 exceedances). The 197 other exceedances are a mix between anthropogenic sources (from 46.3% in MED-We to 80.6% in NEU-We), biogenic sources (12.6% in MED-We to the exceedances of the limitation appears preponderant during the summer of 2012 (from 3530% in NEU-Ce), fires (1.6% in NEU-We to 92.512.4% in MED-We) and mineral dust (4.4% in NEU-We to 13.8% in MED-We). The 25 μg m^{-3} limit recommandation is more often exceeded because of high anthropogenic contributions than natural sources.

Compared to the results without optimization, the main differences are for PM_{10}, with less exceedances due exclusively to dust (197 vs 356) and with a proportion to the 50 μg m^{-3} limit lower (49.5%-67% vs 78.1%-85%). The other sources (anthropogenic, biogenic, fires) are then lower than in the optimized results. This comparison means that the model only is not robust enough to estimate contributions for an air quality purpose for PM_{10}, but can be used as a valuable complement to observations to attribute source.

For $PM_{2.5}$ however, the differences between the contributions deduced from the model only and from the model optimized with the observations are lower (for instance, 64.2%-92.1% vs 46.3%-80.6% for anthropogenic contribution to the 25 μg m^{-3} limit, 1.7%-17.5% vs 4.4%-13.8% for mineral dust contribution), in coherence

with the better agreement of the model in the simulation of $PM_{2.5}$ concentrations.

7 Conclusions

A sensitivity analysis was undertaken over Europe and the Mediterranean region to estimate the contribution of anthropogenic, mineral dust, fire, biogenic and sea salt emissions on surface PM_{10}, surface $PM_{2.5}$ and total AOD during the summer of 2012. Therefore, simulations were performed using the CHIMERE regional CTM, including all sources (reference simulation) and removing one of these source at a time (sensitivity study).

The reference simulation has been evaluated against observations of surface PM from the AirBase network and two more stations in Corsica, and of AOD from the AERONET network and the MODIS space-based instrument. Although the density of the AirBase network is relatively high in parts of Europe, there is ~~a lack of~~ fewer observations around the Mediterranean Basin, which thus ~~cannot be~~ is difficult to evaluated in terms of surface PM concentrations.

For the northern part of the domain and the western Mediterranean Basin, the comparison between CHIMERE simulations and the ~~AirBase observations (~~observations of $PM_{2.5}$ and PM_{10} ~~)~~ surface concentrations has shown the ability of the model to simulate PM levels (the performance criteria are met for hourly values for more than 90% of the stations, i.e. both MFE and MFB are lower than or equal to 75% and ±60% respectively). However, the associated variability is not well established with the correlation ranging from ~~0.38 to 0.49~~ 0.19 to 0.57 depending on the region. All the main peaks are though reproduced by the model. The MFB is under 20% over the area, with some overestimations of peaks in the south west of the domain. The correlation is ~~lower in the~~ the lowest in the south east of the domain, associated with a strong underestimation of the observations, due to missing coarse particles sources, probably mineral dust. In the center north, ~~where local sourcesstrongly influence observations~~statistics give slightly lower coherence with the observations, strongly by local sources. This influence cannot be captured at the resolution used for the simulation (50 km). On the contrary, some peak values are overestimated in the northern part of the domain by up to a factor of 4.

The comparison between simulated AOD and observations from AERONET and MODIS also shows good results with a correlation ranging from ~~0.35 to 0.75~~0.37 to 0.77, and a reasonable MFE (~~36.2~~34.33% with respect to AERONET and ~~24.6~~27.61% with respect to MODIS). ~~An underestimation is seen~~ The underestimation is confirmed in the eastern and southern part of the domain (MFB up to about ~~-39.8~~-31.4%).

Results of sensitivity simulations show that the Euro-Mediterranean domain is strongly influenced by mineral dust transport and anthropogenic emissions (62% and 19% respectively for surface PM_{10} and 17% and 52% for surface $PM_{2.5}$). For mineral dust, the contribution is particularly important in the western Mediterranean Basin (86% for surface PM_{10} and 44% for $PM_{2.5}$) where the concentrations are the highest. In this region, all the extreme peaks are attributed to this source. In the northern part of the domain, mineral dust affects mainly the free troposphere. At the surface, anthropogenic emissions are dominant, particularly for surface $PM_{2.5}$ (up to 75%). However, surface peak concentrations attributed to mineral dust are observed. These peaks are generally strongly overestimated in the simulations. Fire emissions have also a significant contribution (~~up to 20% at the time of the fire~~12.2% in average in MED-Ce) over the Mediterranean Sea, as well as sea salts on surface PM_{10} over coastal cities (29%). Biogenic emissions impact the Central Europe mostly on $PM_{2.5}$ (20%). Although levels of PM in MED-Ea are poorly reproduced in the model, the contribution of anthropogenic emissions on $PM_{2.5}$ (60.7%in average) is coherent with Im and Kanakidou (2012).

Contributions to the total AOD show similar patterns, ~~but~~ except for the contribution of sea ~~salt is very weak due to its low radiative impact and its confinement in the very near surface~~salts which is weaker. Contributions to the total AOD are closest to the ~~distribution of~~ contributions of simulated fine particles ($PM_{2.5}$ from anthropogenic and fire emissions) than coarse ~~, due to the fact that fine particles (for example black carbon) are optically more active at 500 nm,~~ at the wavelength considered ~~here~~in this study (550 nm).

The same analysis was undertaken for the number of stations in daily exceedances of the European Union limit of 50 $\mu g\ m^{-3}$ for PM_{10}, and of the WHO recommendation of 25 $\mu g\ m^{-3}$ for $PM_{2.5}$ (over the ~~AirBase stations). This number is generally~~ stations considered in the study).The number of exceedances is overestimated by the model, mainly because of dust and fire contributions, but exceedances are captured at the right time. ~~The overestimation is most probably due to high concentrations from mineral dust at the surface, and also occurs when diverse sources are mixed. Moreover, if most of the mineral dust outbreaks are well reproduced by the model, the peaks present in the time series of surface PM concentration are strongly overestimated in the northern part of the domain. However, this source is necessary to simulate pollution levels, as the timing and the number of most of the exceedances are not represented if mineral dust emissions are removed. Particularly, natural sources in total are responsible from 35 to 92.5%of the number of stations in daily exceedances depending on the region~~An optimized number of exceedances and associated contributions was computed to estimate more robust contributions to PM_{10} and $PM_{2.5}$ concentrations exceedances. Results show that for PM_{10}, mineral dust and fires can be responsible exclusively of an exceedance (in 35.9% of the cases for mineral dust and 0.7% for fires), whereas it is anthropogenic sources (21.1%) and fires (0.02%) for $PM_{2.5}$. The other exceedances are induced by a mixed

contribution between mainly mineral dust (49.5%-67% for PM_{10} exceedances contributions, 4.4%-13.8% for $PM_{2.5}$), anthropogenic sources (14.9%-24.2% and 46.3%-80.6%), biogenic sources (4.1%-15.7% and 12.6%-30%) and fires (2.2%-7.2% and 1.6%-12.4%). Those results are estimated on average over the western part of Europe and the central north.

Acknowledgements. The authors ~~aknowledge~~ acknowledge financial support from EIT - Climate-KIC as well as from the Centre National d'Etudes Spatiales (CNES) and DGA (in the framework of the APPAD project). Authors are grateful to the EEA for maintaining and providing the AirBase database for surface concentrations of several pollutants over Europe. All investigators and staff who maintain and provide the AERONET data are thanked. We also wish to thank the National Aeronautics and Space Agency (NASA) for the ~~availability~~ availability of the MODIS data.

References

Alfaro, S. C. and Gomes, L.: Modeling mineral aerosol production by wind erosion: Emission intensities and aerosol size distributions in source areas, Journal of Geophysical Research: Atmospheres, 106, 18 075–18 084, doi:10.1029/2000JD900339, 2001.

Anttila, P., Stefanovska, A., Nestorovska-Krsteska, A., Grozdanovski, L., Atanasov, I., Golubov, N., Ristevski, P., Toceva, M., Lappi, S., and Walden, J.: Characterisation of extreme air pollution episodes in an urban valley in the Balkan Peninsula, Air Quality, Atmosphere & Health, pp. 1–13, doi: 10.1007/s11869-015-0326-7, 2015.

Barnaba, F., Angelini, F., Curci, G., and Gobbi, G. P.: An important fingerprint of wildfires on the European aerosol load, Atmospheric Chemistry and Physics, 11, 10 487–10 501, 2011.

Bessagnet, B., Hodzic, A., Vautard, R., Beekmann, M., Cheinet, S., Honoré, C., Liousse, C., and Rouil, L.: Aerosol modeling with CHIMERE: preliminary evaluation at the continental scale, Atmospheric Environment, 38, 2803–2817, doi:10.1016/j.atmosenv.2004.02.034, 2004.

Bian, H., , and Prather, M.: Fast-J2: accurate simulation of stratospheric photolysis in global chemical models, J. Atmos. Chem., 41, 281–296, 2002.

Boldo, E., Medina, S., Le Tertre, A., Hurley, F., Mücke, H.-G., Ballester, F., and Aguilera, I.: Apheis: Health impact assessment of long-term exposure to PM2.5 in 23 European cities, European journal of epidemiology, 21, 449–458, 2006.

Boselli, A., Caggiano, R., Cornacchia, C., Madonna, F., Mona, L., Macchiato, M., Pappalardo, G., and Trippetta, S.: Multi year sun-photometer measurements for aerosol characterization in a Central Mediterranean site, Atmospheric Research, 104, 98–110, 2012.

Boylan, J. W. and Russell, A. G.: PM and light extinction model performance metrics, goals, and criteria for three-dimensional air quality models, Atmospheric Environment, 40, 4946–4959, 2006.

Briant, R., Menut, L., Siour, G., and Prigent, C.: Homogeneized modeling of mineral dust emissions over Europe and Africa using the CHIMERE model, Geoscientific Model Development Discussions, 7, 3441–3480, doi:10.5194/gmdd-7-3441-2014, 2014.

Burr, M., Zhang, Y., et al.: Source apportionment of fine particulate matter over the Eastern US Part II: source apportionment simulations using CAMX/PSAT and comparisons with CMAQ source sensitivity simulations., Atmospheric Pollution Research, 2, 318–336, doi:10.5094/APR.2011.037, 2011.

Carslaw, K., Boucher, O., Spracklen, D., Mann, G., Rae, J., Woodward, S., and Kulmala, M.: A review of natural aerosol interactions and feedbacks within the Earth system, Atmospheric Chemistry and Physics, 10, 1701–1737, 2010.

Curci, G., Palmer, P. I., Kurosu, T. P., Chance, K., and Visconti, G.: Estimating European volatile organic compound emissions using satellite observations of formaldehyde from the Ozone Monitoring Instrument, Atmos. Chem. Phys., 10, 11 501–11 517, 2010.

Curci, G., Hogrefe, C., Bianconi, R., Im, U., Balzarini, A., Baró, R., Brunner, D., Forkel, R., Giordano, L., Hirtl, M., et al.: Uncertainties of simulated aerosol optical properties induced by assumptions on aerosol physical and chemical properties: An AQMEII-2 perspective, Atmospheric Environment, doi:10.1016/j.atmosenv.2014.09.009, 2014.

DallOsto, M., Harrison, R. M., Highwood, E. J., ODowd, C., Ceburnis, D., Querol, X., and Achterberg, E. P.: Variation of the mixing state of Saharan dust particles with atmospheric transport, Atmospheric Environment, 44, 3135–3146, 2010.

Daskalakis, N., Myriokefalitakis, S., and Kanakidou, M.: Sensitivity of tropospheric loads and lifetimes of short lived pollutants to fire emissions, Atmospheric Chemistry and Physics Discussions, 14, 22 639–22 676, 2014.

Dubovik, O., Smirnov, A., Holben, B., King, M., Kaufman, Y., Eck, T., and Slutsker, I.: Accuracy assessments of aerosol optical properties retrieved from Aerosol Robotic Network (AERONET) Sun and sky radiance measurements, Journal of Geophysical Research: Atmospheres (1984–2012), 105, 9791–9806, 2000.

Dudhia, J.: Numerical study of convection observed during the winter monsoon experiment using a mesoscale two-dimensional model, Journal of the Atmospheric Sciences, 46, 3077–3107, 1989.

Fecan, F., Marticorena, B., and Bergametti, G.: Parameterization of the increase of aeolian erosion threshold wind friction velocity due to soil moisture for arid and semi-arid areas, Annals of Geophysics, 17, 149–157, 1999.

Folberth, G. A., Hauglustaine, D. A., Lathière, J., and Brocheton, F.: Interactive chemistry in the Laboratoire de Météorologie Dynamique general circulation model: model description and impact analysis of biogenic hydrocarbons on tropospheric chemistry, Atmos. Chem. Phys., 6, 2273–2319, 2006.

Gerasopoulos, E., Kouvarakis, G., Babasakalis, P., Vrekoussis, M., Putaud, J.-P., and Mihalopoulos, N.: Origin and variability of particulate matter (PM_{10}) mass concentrations over the Eastern Mediterranean, Atmospheric Environment, 40, 4679–4690, 2006.

Gerasopoulos, E., Amiridis, V., Kazadzis, S., Kokkalis, P., Eleftheratos, K., Andreae, M., Andreae, T., El-Askary, H., and Zerefos, C.: Three-year ground based measurements of aerosol optical depth over the Eastern Mediterranean: the urban environment of Athens, Atmospheric Chemistry and Physics, 11, 2145–2159, 2011.

Ginoux, P., Chin, M., Tegen, I., Prospero, J. M., Holben, B., Dubovik, O., and Lin, S. J.: Sources and distributions of dust aerosols simulated with the GOCART model, Journal of Geo-

physical Research, 106, 20 255–20 273, 2001.

Gobbi, G., Barnaba, F., and Ammannat, L.: Estimating the impact of Saharan dust on the year 2001 PM10 record of Rome, Italy, Atmospheric Environment, 41, 261–275, 2007.

Gómez-Amo, J., Estellés, V., Segura, S., Marcos, C., Esteve, A., Pedrós, R., Utrillas, M., and Martínez-Lozano, J.: Analysis of a strong wildfire event over Valencia (Spain) during Summer 2012–Part 1: Aerosol microphysics and optical properties, Atmospheric Chemistry and Physics Discussions, 13, 22 639–22 685, 2013.

Guenther, A., Karl, T., Harley, P., Wiedinmyer, C., Palmer, P., and Geron, C.: Estimates of global terrestrial isoprene emissions using MEGAN (Model of Emissions of Gases and Aerosols from Nature), Atmos. Chem. Phys., 6, 3181–3210, 2006.

Hansen, J., Sato, M., and Ruedy, R.: Radiative forcing and climate response, Journal of Geophysical Research: Atmospheres, 102, 6831–6864, doi:10.1029/96JD03436, 1997.

Hodzic, A., Madronich, S., Bohn, B., Massie, S., Menut, L., and Wiedinmyer, C.: Wildfire particulate matter in Europe during summer 2003: Meso-scale modeling of smoke emissions, transport and radiative effects, Atmospheric Chemistry and Physics, 7, 2007.

Holben, B., Eck, T., Slutsker, I., Tanré, D., Buis, J., Setzer, A., Vermote, E., Reagan, J., Kaufman, Y., Nakajima, T., Lavenu, F., Jankowiak, I., and Smirnov, A.: AERONET - A federated instrument network and data archive for aerosol characterization, Remote sensing of environment, 66, 1–16, 1998.

Hong, S.-Y. and Lim, J.-O. J.: The WRF single-moment 6-class microphysics scheme (WSM6), J. Korean Meteor. Soc, 42, 129–151, 2006.

Iacono, M. J., Delamere, J. S., Mlawer, E. J., Shephard, M. W., Clough, S. A., and Collins, W. D.: Radiative forcing by long-lived greenhouse gases: Calculations with the AER radiative transfer models, Journal of Geophysical Research: Atmospheres (1984–2012), 113, 2008.

Im, U. and Kanakidou, M.: Impacts of East Mediterranean megacity emissions on air quality, Atmospheric Chemistry and Physics, 12, 6335–6355, doi:10.5194/acp-12-6335-2012, 2012.

Im, U., Bianconi, R., Solazzo, E., Kioutsioukis, I., Badia, A., Balzarini, A., Baró, R., Bellasio, R., Brunner, D., Chemel, C., Curci, G., Denier van der Gon, H., Flemming, J., Forkel, R., Giordano, L., Jiménez-Guerrero, P., Hirtl, M., Hodzic, A., Honzak, L., Jorba, O., Knote, C., Makar, P., Manders-Groot, A., Neal, L., Pérez, J., Pirovano, G., Pouliot, G., San Jose, R., Savage, N., Schroder, W., Sokhi, R., Syrakov, D., Torian, A., Tuccella, P., Wang, K., Werhahn, J., Wolke, R., Zabkar, R., Zhang, Y., Zhang, J., Hogrefe, C., and Galmarini, S.: Evaluation of operational online-coupled regional air quality models over Europe and North America in the context of AQMEII phase 2. Part II: Particulate matter, Atmospheric Environment, doi:10.1016/j.atmosenv.2014.08.072, 2014.

Israelevich, P., Ganor, E., Alpert, P., Kishcha, P., and Stupp, A.: Predominant transport paths of Saharan dust over the Mediterranean Sea to Europe, Journal of Geophysical Research: Atmospheres, 117, n/a–n/a, doi:10.1029/2011JD016482, 2012.

Israelevich, P. L., Levin, Z., Joseph, J. H., and Ganor, E.: Desert aerosol transport in the Mediterranean region as inferred from the TOMS aerosol index, Journal of Geophysical Research: Atmospheres, 107, AAC 13–1–AAC 13–13, doi:10.1029/2001JD002011, 2002.

Janjic, Z.: The surface layer parameterization in the NCEP Eta Model, WORLD METEOROLOGICAL ORGANIZATION-PUBLICATIONS-WMO TD, pp. 4–16, 1996.

Kain, J. S.: Convective parameterization for mesoscale models: The Kain–Fritsch scheme, The representation of cumulus convection in numerical models, Meteor. Monogr, 46, 165–170, 1993.

Kalnay, E., Kanamitsu, M., Kistler, R., Collins, W., Deaven, D., Gandin, L., Iredell, M., Saha, S., White, G., Woollen, J., Zhu, Y., Chelliah, M., Ebisuzaki, W., Higgins, W., Janowiak, J., Mo, K., Ropelewski, C., Wang, J., Leetmaa, A., Reynolds, R., Jenne, R., and Joseph, D.: The NCEP/NCAR 40-year reanalysis project, Bull. Amer. Meteorol. Soc., pp. 437–471, 1996.

Kaskaoutis, D., Kambezidis, H., Nastos, P., and Kosmopoulos, P.: Study on an intense dust storm over Greece, Atmospheric Environment, 42, 6884–6896, 2008.

Katsouyanni, K., Touloumi, G., Spix, C., Schwartz, J., Balducci, F., Medina, S., Rossi, G., Wojtyniak, B., Sunyer, J., Bacharova, L., Schouten, J. P., Ponka, A., and Anderson, H. R.: Short term effects of ambient sulphur dioxide and particulate matter on mortality in 12 European cities: results from time series data from the APHEA project, BMJ, 314, 1658, doi:10.1136/bmj.314.7095.1658, 1997.

Koçak, M., Mihalopoulos, N., and Kubilay, N.: Contributions of natural sources to high PM_{10} and $PM_{2.5}$ events in the eastern Mediterranean, Atmospheric Environment, 41, 3806–3818, 2007.

Koo, B., Dunker, A. M., and Yarwood, G.: Implementing the Decoupled Direct Method for Sensitivity Analysis in a Particulate Matter Air Quality Model, Environmental Science & Technology, 41, 2847–2854, doi:10.1021/es0619962, pMID: 17533848, 2007.

Koo, B., Wilson, G. M., Morris, R. E., Dunker, A. M., and Yarwood, G.: Comparison of source apportionment and sensitivity analysis in a particulate matter air quality model, Environmental science & technology, 43, 6669–6675, doi:10.1021/es9008129, 2009.

Lionello, P., Malanotte-Rizzoli, P., Boscolo, R., Alpert, P., Artale, V., Li, L., Luterbacher, J., May, W., Trigo, R., Tsimplis, M., Ulbrich, U., and Xoplaki, E.: The Mediterranean climate: an overview of the main characteristics and issues, Developments in earth and environmental sciences, 4, 1–26, 2006.

Mailler, S., Menut, L., Di Sarra, A. G., Becagli, S., Di Iorio, T., Formenti, P., Bessagnet, B., Briant, R., Gmez-Amo, J. L., Mallet, M., Rea, G., Siour, G., Sferlazzo, D. M., Traversi, R., Udisti, R., and Turquety, S.: On the radiative impact of aerosols on photolysis rates: comparison of simulations and observations in the Lampedusa island during the CharMEx/ADRIMED campaign, Atmospheric Chemistry and Physics, submitted.

Marticorena, B. and Bergametti, G.: Modeling the atmospheric dust cycle: 1. Design of a soil-derived dust emission scheme, Journal of Geophysical Research: Atmospheres, 100, 16 415–16 430, doi:10.1029/95JD00690, 1995.

Menut, L., Schmechtig, C., and Marticorena, B.: Sensitivity of the sandblasting fluxes calculations to the soil size distribution accuracy, Journal of Atmospheric and Oceanic Technology, 22, 1875–1884, doi:10.1175/JTECH1825.1, 2005.

Menut, L., Foret, G., and Bergametti, G.: Sensitivity of mineral dust concentrations to the model size distribution accuracy, Journal of Geophysical Research, Atmospheres, 112, D10 210, doi:10.

1029/2006JD007766, 2007.

Menut, L., Chiapello, I., and Moulin, C.: Previsibility of mineral dust concentrations: The CHIMERE-DUST forecast during the first AMMA experiment dry season, J. Geophys. Res., 114, D07 202, doi:10.1029/2008JD010523, 2009.

Menut, L., Goussebaile, A., Bessagnet, B., Khvorostiyanov, D., and Ung, A.: Impact of realistic hourly emissions profiles on air pollutants concentrations modelled with CHIMERE, Atmospheric Environment, 49, 233–244, doi:10.1016/j.atmosenv.2011.11.057, 2012.

Menut, L., Bessagnet, B., Khvorostyanov, D., Beekmann, M., Blond, N., Colette, A., Coll, I., Curci, G., Foret, G., Hodzic, A., Mailler, S., Meleux, F., Monge, J., Pison, I., Siour, G., Turquety, S., Valari, M., Vautard, R., and Vivanco, M.: CHIMERE 2013: a model for regional atmospheric composition modelling, Geoscientific Model Development, 6, 981–1028, doi:10.5194/gmd-6-981-2013, 2013.

Menut, L., Mailler, S., Siour, G., Bessagnet, B., Turquety, S., G., R., Briant, R., Mallet, M., Sciare, J., and P., F.: Ozone and aerosols tropospheric concentrations variability analyzed using the ADRIMED measurements and the WRF-CHIMERE models, Atmospheric Chemistry and Physics, submitted.

Millán, M. M., José Sanz, M., Salvador, R., and Mantilla, E.: Atmospheric dynamics and ozone cycles related to nitrogen deposition in the western Mediterranean, Environmental Pollution, 118, 167–186, 2002.

Monahan, E. C.: In The Role of Air-Sea Exchange in Geochemical Cycling, chap. The ocean as a source of atmospheric particles, pp. 129–163, Kluwer Academic Publishers, Dordrecht, Holland, 1986.

Monks, P., Granier, C., Fuzzi, S., Stohl, A., Williams, M., Akimoto, H., Amann, M., Baklanov, A., Baltensperger, U., Bey, I., Blake, N., Blake, R., Carslaw, K., Cooper, O., Dentener, F., Fowler, D., Fragkou, E., Frost, G., Generoso, S., Ginoux, P., Grewe, V., Guenther, A., Hansson, H., Henne, S., Hjorth, J., Hofzumahaus, A., Huntrieser, H., Isaksen, I., Jenkin, M., Kaiser, J., Kanakidou, M., Klimont, Z., Kulmala, M., Laj, P., Lawrence, M., Lee, J., Liousse, C., Maione, M., McFiggans, G., Metzger, A., Mieville, A., Moussiopoulos, N., Orlando, J., O'Dowd, C., Palmer, P., Parrish, D., Petzold, A., Platt, U., Pschl, U., Prvt, A., Reeves, C., Reimann, S., Rudich, Y., Sellegri, K., Steinbrecher, R., Simpson, D., ten Brink, H., Theloke, J., van der Werf, G., Vautard, R., Vestreng, V., Vlachokostas, C., and von Glasow, R.: Atmospheric composition change - global and regional air quality, Atmospheric Environment, 43, 5268 – 5350, doi:10.1016/j.atmosenv.2009.08.021, 2009.

Moulin, C., Lambert, C. E., Dayan, U., Masson, V., Ramonet, M., Bousquet, P., Legrand, M., Balkanski, Y. J., Guelle, W., Marticorena, B., Bergametti, G., and Dulac, F.: Satellite climatology of African dust transport in the Mediterranean atmosphere, Journal of Geophysical Research: Atmospheres, 103, 13 137–13 144, doi:10.1029/98JD00171, 1998.

Nabat, P., Somot, S., Mallet, M., Chiapello, I., Morcrette, J. J., Solmon, F., Szopa, S., Dulac, F., Collins, W., Ghan, S., Horowitz, L. W., Lamarque, J. F., Lee, Y. H., Naik, V., Nagashima, T., Shindell, D., and Skeie, R.: A 4-D climatology (1979-2009) of the monthly tropospheric aerosol optical depth distribution over the Mediterranean region from a comparative evaluation and blending of remote sensing and model products, Atmospheric Measurement Techniques, 6, 1287–1314, doi:10.5194/amt-6-1287-2013, 2013.

Nabat, P., Somot, S., Mallet, M., Michou, M., Sevault, F., Driouech, F., Meloni, D., di Sarra, A., Di Biagio, C., Formenti, P., Sicard, M., Léon, J.-F., and Bouin, M.-N.: Dust aerosol radiative effects during summer 2012 simulated with a coupled regional aerosol-atmosphere-ocean model over the Mediterranean, Atmospheric Chemistry and Physics, 15, 3303–3326, doi:10.5194/acp-15-3303-2015, 2015.

Pace, G., Meloni, D., and di Sarra, A.: Forest fire aerosol over the Mediterranean basin during summer 2003, Journal of Geophysical Research: Atmospheres, 110, n/a–n/a, doi:10.1029/2005JD005986, 2005.

Péré, J., Mallet, M., Pont, V., and Bessagnet, B.: Evaluation of an aerosol optical scheme in the chemistry-transport model CHIMERE, Atmospheric Environment, 44, 3688–3699, doi:10.1016/j.atmosenv.2010.06.034, 2010.

Pope III, C. A. and Dockery, D. W.: Health effects of fine particulate air pollution: lines that connect, Journal of the Air & Waste Management Association, 56, 709–742, 2006.

Prigent, C., Jiménez, C., and Catherinot, J.: Comparison of satellite microwave backscattering (ASCAT) and visible/near-infrared reflectances (PARASOL) for the estimation of aeolian aerodynamic roughness length in arid and semi-arid regions, Atmos. Meas. Tech., 5, 2703–2712, 2012.

Prospero, J. M., Ginoux, P., Torres, O., Nicholson, S. E., and Gill, T. E.: ENVIRONMENTAL CHARACTERIZATION OF GLOBAL SOURCES OF ATMOSPHERIC SOIL DUST IDENTIFIED WITH THE NIMBUS 7 TOTAL OZONE MAPPING SPECTROMETER (TOMS) ABSORBING AEROSOL PRODUCT, Reviews of Geophysics, 40, 2–1–2–31, doi:10.1029/2000RG000095, 2002.

Putaud, J.-P., Van Dingenen, R., Alastuey, A., Bauer, H., Birmili, W., Cyrys, J., Flentje, H., Fuzzi, S., Gehrig, R., Hansson, H.-C., et al.: A European aerosol phenomenology–3: Physical and chemical characteristics of particulate matter from 60 rural, urban, and kerbside sites across Europe, Atmospheric Environment, 44, 1308–1320, 2010.

Remer, L. A., Kaufman, Y. J., Tanré, D., Mattoo, S., Chu, D. A., Martins, J. V., Li, R.-R., Ichoku, C., Levy, R. C., Kleidman, R. G., Eck, T. F., Vermote, E., and Holben, B. N.: The MODIS Aerosol Algorithm, Products and Validation, Special Section, Journal of the Atmospheric Sciences, 62, 947–973, 2005.

Remer, L. A., Tanre, D., Kaufman, Y. J., Levy, R., and Mattoo, S.: Algorithm for remote sensing of tropospheric aerosol from MODIS: Collection 005, National Aeronautics and Space Administration, 2006.

Ripoll, A., Minguillón, M. C., Pey, J., Pérez, N., Querol, X., and Alastuey, A.: Joint analysis of continental and regional background environments in the western Mediterranean: PM_1 and PM_{10} concentrations and composition, Atmospheric Chemistry and Physics, 15, 1129–1145, doi:10.5194/acp-15-1129-2015, 2015.

Rodriguez, S., Querol, X., Alastuey, A., and de la Rosa., J.: Atmospheric particulate matter and air quality in the Mediterranean: a review, Environmental Chemistry Letters, 5, 1–7, doi:10.1007/s10311-006-0071-0, 2007.

Roustan, Y., Sartelet, K., Tombette, M., Debry, É., and Sportisse, B.: Simulation of aerosols and gas-phase species over Europe

with the POLYPHEMUS system. Part II: Model sensitivity analysis for 2001, Atmospheric Environment, 44, 4219–4229, 2010.

Salvador, P., Alonso, S., Pey, J., Artíñano, B., de Bustos, J., Alastuey, A., and Querol, X.: African dust outbreaks over the western Mediterranean basin: 11 year characterization of atmospheric circulation patterns and dust source areas, Atmospheric Chemistry and Physics Discussions, 14, 5495–5533, 2014.

Sartelet, K. N., Couvidat, F., Seigneur, C., and Roustan, Y.: Impact of biogenic emissions on air quality over Europe and North America, Atmospheric Environment, 53, 131–141, 2012.

Sayer, A. M., Hsu, N. C., Bettenhausen, C., and Jeong, M.-J.: Validation and uncertainty estimates for MODIS collection 6 "Deep Blue" aerosol data, J. Geophys. Res. Atmospheres, 118, 7864–7872, 2013.

Skamarock, W., Klemp, J., Dudhia, J., Gill, D., Barker, D., Duda, M., Huang, X., Wang, W., and Powers, J.: A description of the advanced research WRF version 3., NCAR Technical Note, p. 123pp, 2008.

Solazzo, E., Bianconi, R., Pirovano, G., Matthias, V., Vautard, R., Moran, M. D., Appel, K. W., Bessagnet, B., Brandt, J., Christensen, J. H., Chemel, C., Coll, I., Ferreira, J., Forkel, R., Francis, X. V., Grell, G., Grossi, P., Hansen, A. B., Miranda, A. I., Nopmongcol, U., Prank, M., Sartelet, K. N., Schaap, M., Silver, J. D., Sokhi, R. S., Vira, J., Werhahn, J., Wolke, R., Yarwood, G., Zhang, J., Rao, S. T., and Galmarini, S.: Operational model evaluation for particulate matter in Europe and North America in the context of AQMEII, Atmospheric Environment, 53, 75 – 92, doi:10.1016/j.atmosenv.2012.02.045, 2012.

Stocker, T., Qin, D., Plattner, G., Tignor, M., Allen, S., Boschung, J., Nauels, A., Xia, Y., Bex, V., and Midgley, P.: Climate change 2013: the physical science basis. Contribution of Working Group I to the Fifth Assessment Report of the Intergovernmental Panel on Climate Change, 2013.

Textor, C., Schulz, M., Guibert, S., Kinne, S., Balkanski, Y., Bauer, S., Berntsen, T., Berglen, T., Boucher, O., Chin, M., Dentener, F., Diehl, T., Easter, R., Feichter, H., Fillmore, D., Ghan, S., Ginoux, P., Gong, S., Grini, A., Hendricks, J., Horowitz, L., Huang, P., Isaksen, I., Iversen, I., Kloster, S., Koch, D., Kirkevåg, A., Kristjansson, J. E., Krol, M., Lauer, A., Lamarque, J. F., Liu, X., Montanaro, V., Myhre, G., Penner, J., Pitari, G., Reddy, S., Seland, Ø., Stier, P., Takemura, T., and Tie, X.: Analysis and quantification of the diversities of aerosol life cycles within AeroCom, Atmospheric Chemistry and Physics, 6, 1777–1813, doi:10.5194/acp-6-1777-2006, 2006.

Turquety, S., Menut, L., Bessagnet, B., Anav, A., Viovy, N., Maignan, F., and Wooster, M.: APIFLAME v1.0: High resolution fire emission model and application to the Euro-Mediterranean region, Geoscientific Model Development, 7, 587–612, doi:10.5194/gmd-7-587-2014, 2014.

Vuolo, M. R., Chepfer, H., Menut, L., and Cesana, G.: Comparison of mineral dust layers vertical structures modeled with CHIMERE-DUST and observed with the CALIOP lidar, Journal of Geophysical Research: Atmospheres, 114, doi:10.1029/2008JD011219, 2009.

Wild, O., Zhu, X., and Prather, J.: Fast-J: accurate simulation of the in- and below-cloud photolysis in tropospheric chemical models, J. Atmos. Chem., 37, 245–282, 2000.

Yu, H., Kaufman, Y. J., Chin, M., Feingold, G., Remer, L. A., Anderson, T. L., Balkanski, Y., Bellouin, N., Boucher, O., Christopher, S., DeCola, P., Kahn, R., Koch, D., Loeb, N., Reddy, M. S., Schulz, M., Takemura, T., and Zhou, M.: A review of measurement-based assessments of the aerosol direct radiative effect and forcing, Atmospheric Chemistry and Physics, 6, 613–666, doi:10.5194/acp-6-613-2006, 2006.